SCIENCE CHINA
Earth Sciences

•REVIEW•

May 2023 Vol.66 No.5: 939–958
https://doi.org/10.1007/s11430-022-1092-y

COATS: Comprehensive observation on the atmospheric boundary layer three-dimensional structure during haze pollution in the North China Plain

Qianhui LI[1,2], Hongsheng ZHANG[2*], Xiaoye ZHANG[3†], Xuhui CAI[4], Xipeng JIN[4], Lu ZHANG[2], Yu SONG[4], Ling KANG[4], Fei HU[5] & Tong ZHU[4]

[1] *Tianjin Key Laboratory for Oceanic Meteorology, Tianjin Meteorological Service Center, Tianjin Meteorological Bureau, Tianjin 300074, China;*
[2] *Laboratory for Climate and Ocean-Atmosphere Studies, Department of Atmospheric and Oceanic Sciences, School of Physics, Peking University, Beijing 100871, China;*
[3] *State Key Laboratory of Severe Weather and Key Laboratory of Atmospheric Chemistry of CMA, Chinese Academy of Meteorological Sciences, China Meteorological Administration (CMA), Beijing 100081, China;*
[4] *State Key Joint Laboratory of Environmental Simulation and Pollution Control, College of Environmental Sciences and Engineering, Peking University, Beijing 100871, China;*
[5] *State Key Laboratory of Atmospheric Boundary Layer Physics and Atmospheric Chemistry, Institute of Atmospheric Physics, Chinese Academy of Sciences, Beijing 100029, China*

Received September 28, 2022; revised February 14, 2023; accepted March 20, 2023; published online April 23, 2023

Abstract The North China Plain (NCP) is troubled by severe haze pollution and the evolution of haze pollution is closely related to the atmospheric boundary layer (ABL). However, experimental and theoretical studies on the physical-chemical processes of the ABL in the NCP are lacking, with many scientific problems to be addressed. To solve these problems, the Comprehensive Observation on the Atmospheric boundary layer Three-dimensional Structure (COATS) during haze pollution was carried out in the NCP from 2016 to 2020. The COATS experiment adopted a "point-line-surface" spatial layout, obtaining both spatial-temporal profiles of the meteorological and environmental elements in the ABL and the turbulent transport data of fine particulate matter ($PM_{2.5}$) in winter and summer. The research achievements are as follows. The spatial-temporal distribution characteristics of the ABL structure and $PM_{2.5}$ concentrations in the NCP were determined. The typical thermal structure of persistent heavy haze events and the pollutant removal mechanism by low-level jets were revealed. It was determined that the spatial structure of the ABL adjusted by the Taihang Mountains is responsible for the heterogeneous distribution of haze pollution in the NCP, and that mountain-induced vertical circulations can promote the formation of elevated pollution layers. The restraints of the atmospheric internal boundaries on horizontal diffusion of pollutants were emphasized. The contribution of the ABL to haze pollution in winter and summer was qualitatively compared and quantitatively estimated. The turbulent transport nature behind the relationship between the atmospheric boundary layer height (ABLH) and surface $PM_{2.5}$ concentrations was analyzed. The concept of "aerosol accumulation layer" was defined, and the applicability of the material method in determining ABLH was clarified. A measurement system for obtaining the turbulent flux of $PM_{2.5}$ concentrations was developed, and the turbulence characteristics of $PM_{2.5}$ concentrations were demonstrated. The COATS experiment is of great theoretical significance for thoroughly understanding the physical mechanisms of the ABL during haze pollution and filling the knowledge gap on the impacts of the ABL three-dimensional structure on haze pollution. The results of this study are conducive to the improvement and development of ABL parameterization schemes and serve as a scientific basis for formulating regional pollution prevention and control measures.

* Corresponding author (email: hsdq@pku.edu.cn)
† Corresponding author (email: xiaoye@cma.gov.cn)

Keywords COATS experiment, Haze pollution, ABL three-dimensional structure, Aerosol accumulation layer, Turbulent flux of $PM_{2.5}$ concentrations, North China Plain

Citation: Li Q, Zhang H, Zhang X, Cai X, Jin X, Zhang L, Song Y, Kang L, Hu F, Zhu T. 2023. COATS: Comprehensive observation on the atmospheric boundary layer three-dimensional structure during haze pollution in the North China Plain. Science China Earth Sciences, 66(5): 939–958, https://doi.org/10.1007/s11430-022-1092-y

1. Introduction

Haze events frequently occur in the North China Plain (NCP), one of the regions with the most severe haze pollution in China (Fan et al., 2020; Guo et al., 2020). The evolution of the atmospheric boundary layer (ABL) structure directly affects the diffusion and transport of pollutants between the ground and atmosphere and controls the chemical transformations of aerosols. The ABL plays a critical role in the generation and dissipation of haze pollution, and influence the accumulation of pollutants. Thus, the interaction between the ABL and haze pollution has attracted extensive attention among researchers (Zhong et al., 2018a; Miao et al., 2019). The NCP is bounded by the Taihang Mountains and Yanshan Mountains to the west and north and is adjacent to the Bohai Sea to the east. Due to orographic forcing and the differences in thermal properties between land and sea, the meteorological conditions of the ABL in the NCP are spatially heterogeneous, with complex mountain-plain wind patterns and sea-land wind circulations. The haze pollution in the NCP is often characterized by long duration, regionality, spatial heterogeneity, and explosive growth in pollutant concentrations (Guo et al., 2014; Li et al., 2015; Bei et al., 2017, 2020; Cai et al., 2017; Zhong et al., 2018b).

Many field experiments have been conducted on aerosol physical properties, chemical transformation mechanisms, and turbulent transport patterns in the NCP with the support of the National Natural Science Foundation of China and the National Key Research and Development Program of China, aiming to clarify the physical-chemical processes within the ABL and their interactions with haze pollution (Wang et al., 2015; Quan et al., 2020). For instance, long-term observations on gradients of meteorological elements, pollutants, and atmospheric turbulence have been performed based on the platforms of the 325 m meteorological tower in Beijing and 255 m meteorological tower in Tianjin to analyze the turbulent transport of pollutants (Qu et al., 2014; Li et al., 2018). From 2001 to 2003, the Chinese Academy of Meteorological Sciences led the "Beijing City Air Pollution Experiment" explored the structural characteristics and physical-chemical processes of the ABL during haze pollution, depicting comprehensive physical images of the "air dome" (Xu et al., 2004, 2006). In 2006, Peking University organized the international cooperative research program "Campaign of Air Quality Research in Beijing and Surrounding Region" to investigate the physical-chemical properties, chemical transformations, and health impacts of aerosols (Liu et al., 2009; van Pinxteren et al., 2009). The field experiment "Haze in China", conducted in the northern part of the NCP in 2009, focused on the optical properties, hygroscopicity, and radiative effects of aerosols, and improved the aerosol parameterization scheme (Ma et al., 2011; Chen et al., 2012; Deng et al., 2013). From 2015 to 2017, the Institute of Urban Meteorology, China Meteorological Administration, organized the "Study of Urban Impacts on Rainfall and Fog/Haze" in the Beijing-Tianjin-Hebei region. The sources, transport processes, and chemical transformations of aerosols during the winter haze pollution periods in Beijing were analyzed in detail with comprehensive observations of the ABL, atmospheric turbulence, and particulate matter concentrations (Liang et al., 2018). The "Multiphase chemistry experiment in Fogs and Aerosols in the North China Plain" was carried out in Gucheng, Hebei Province, China, from 2017 to 2018, and enhanced the understanding of the physical-chemical mechanisms for aerosol generation, especially the contribution of heterogeneous chemical reactions to fog-haze weather (Li G et al., 2021). In the winter of 2018, multi-platform cooperative observations on atmospheric pollutants under the project "vertical detection technologies for air pollution in the terrestrial planetary boundary layer" funded by the National Key Research and Development Program of China were conducted in the Beijing-Tianjin-Hebei region. The influence of the ABL structure on pollutant transport and diffusion in the NCP was explored using a combination of single-station, fixed-point observations with tethered balloons, and meteorological towers, and cruise observations with fixed-wing aircraft and LiDAR (Liu et al., 2019; Sun et al., 2021).

Although previous studies have enriched our understanding of the physical-chemical processes in the ABL during haze pollution, experimental measurements and theoretical studies still have many limitations. For field observations, there have been few reports on high-resolution simultaneous observations of the vertical distribution of the ABL meteorological elements and pollutants. Complete physical images reflecting boundary layer processes during haze pollution cannot be captured through ground-based or meteorological tower-based observations, making it difficult to analyze the transport and diffusion of pollutants in the entire ABL, especially the upper ABL. Theoretical studies mainly focus on describing the ABL structure during haze pollution, yet the influencing mechanism of the evolution of

the ABL structure on the vertical distribution of pollutants needs to be further explored (Liu et al., 2015; Peng et al., 2016; Li et al., 2019). In the NCP, persistent heavy haze pollution also occurs in summer (Cao et al., 2015; Xu et al., 2020). However, studies on summertime haze pollution were rare and available studies primarily focused on the physical-chemical properties of aerosols. Thus, we still have little knowledge of the meteorological mechanisms of the ABL under haze conditions in summer. The Taihang Mountains have an adjusting effect on the meteorological conditions of the ABL in the NCP, resulting in the heterogeneous spatial distribution of haze pollution, and the polluted air masses usually have distinct boundaries (Zou et al., 2018; Yu et al., 2019; Jin et al., 2022a). Most experimental studies on haze pollution in the NCP are based on single-station measurements, so it is difficult to understand the entire ABL spatial structure or the complete spatial distribution pattern of haze pollution. The impact of the heterogenous spatial structure of the ABL and complex local circulations on haze pollution distribution in the mountain front regions of the NCP is still not clear, and the unique phenomenon of the polluted air masses is not yet elucidated. The LiDAR-based boundary layer inversion method has been widely applied, but the inversion results often differ from the conventional concept of the ABL (Shi et al., 2020; Su et al., 2020). The applicability and physical significance of the material method to determine the atmospheric boundary layer height (ABLH) need to be further elucidated. In addition, there have been few reports on experimental measurements of turbulent fluxes of pollutants, and there is a knowledge gap on the turbulent transport characteristics of fine particulate matter ($PM_{2.5}$) (Ren et al., 2019a). Due to the insufficient understanding of local-scale physical processes in the ABL and local circulation patterns at the mountain front, as well as the unclear turbulent transport pattern of particulate matter, it is difficult to simulate heavy haze pollution events accurately using air quality models (Wang et al., 2014; Liang et al., 2018).

Given the above scientific problems, Peking University, together with the Chinese Academy of Meteorological Sciences and the Institute of Atmospheric Physics, Chinese Academy of Sciences, carried out the experiment "Comprehensive Observation on the Atmospheric boundary layer Three-dimensional Structure" (COATS) during haze pollution in the NCP from 2016 to 2020. This experiment aims to deeply reveal the influencing mechanisms of the ABL on haze pollution processes, investigate the impact of heterogenous boundary layer structure on the spatial-temporal distribution of haze pollution, clarify the effects of seasonal variations of the boundary layer meteorology on haze pollution, determine the ABLH more accurately and obtain the turbulent transport features of $PM_{2.5}$. The COATS experiment periods covered winter and summer seasons, with a "point-line-surface" spatial layout. As the vertical profiling of the ABL was combined with ground-based observations, the meteorological and environmental element profiles of the ABL in the NCP in different seasons and the $PM_{2.5}$ turbulent transport data were comprehensively obtained. The results provided valuable data for studying the ABL, weather, and climatic conditions in the NCP and enriched our understanding of the ABL three-dimensional structure in the NCP and its influences on haze pollution. These results are of great theoretical significance for properly understanding the mechanisms of the ABL structure evolution on haze generation, accumulation, and dissipation. This study facilitates the improvement and development of the ABL parameterization scheme applicable to haze pollution periods, and provides an observation basis for correcting the biases of haze pollution simulations using air quality models, which is critical for raising air quality forecasting capacity. It also provides a scientific basis for formulating air pollution prevention and control measures in the NCP region.

2. COATS experiment layout

The design of the COATS experiment was based on numerical modeling results from previous studies, which showed that the air pollution potential tends to increase from the northwest to the southeast of the NCP and that potential source area (footprint) of persistent heavy haze pollution tends to spread along the Taihang Mountains toward the southwest (Zou et al., 2018; Yu et al., 2019). Attracted by the spatial heterogeneity of the ABL structure and the distribution of haze pollution in front of the Taihang Mountains, researchers designed the COATS experiment as follows. In terms of observation methods, the experiment adopted a newly developed sounding system that contains a particulate concentration sensor so that profiles of meteorological elements and $PM_{2.5}$ concentrations can be measured simultaneously. At the same time, atmospheric turbulence and radiation measurements were carried out at the ground level to obtain the turbulent transport features of heat, moisture, energy, and $PM_{2.5}$ in the surface layer. According to the experimental design, the COATS experiment was implemented step by step, with a total of three stages: "point", "line", and "surface". The "point-line-surface" layout of the COATS experiment is illustrated in Figure 1. First, from 2016 to 2018, multiple phases of "point" experiments were conducted at pre-existing experimental bases of Cangzhou and Dezhou, during which the observation instruments were tested, the technique to measure the profiles of meteorological elements and $PM_{2.5}$ concentrations using the newly developed particulate sounding system was proved to be mature, and the basic structural characteristics of the ABL in the NCP were obtained. On this basis, the "line" experiment was implemented in the summer of 2019, with observations

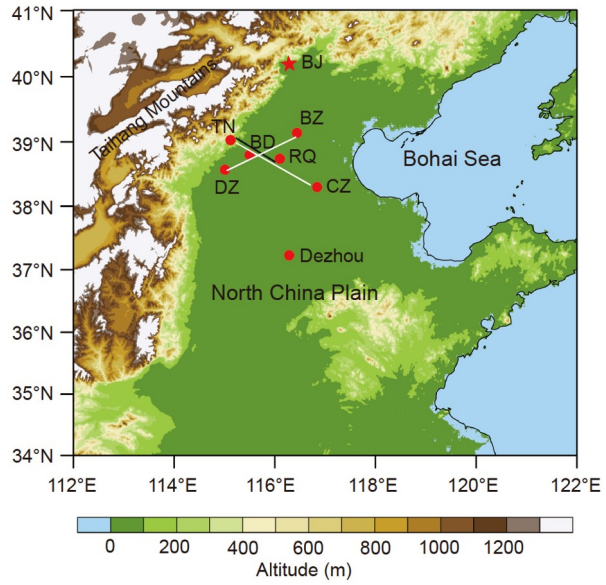

Figure 1 Distribution of COATS experimental stations in the NCP. BJ: Beijing; TN: Tuonan; BD: Baoding; RQ: Renqiu; CZ: Cangzhou; BZ: Bazhou; DZ: Dingzhou.

simultaneously performed at three stations in front of the Taihang Mountains to examine the reasonability of the observation site layout and the reliability of the systematic particulate sounding system. With Baoding station, a pollution center at the mountain front, as the center, Renqiu and Tuonan stations were established at about 50 km to its east and west. Experimental results have shown that the spatial heterogeneity of the ABL can be successfully captured with such a station spacing, and the contribution of the ABL to persistent haze pollution in summer was investigated. Based on the "line" experiment, a "surface" experiment with an observation network consisting of six stations was implemented in the winter of 2019. The cross-shaped observation network was centered at Baoding and the spacing between adjacent stations was about 50–80 km. The three-dimensional structural image of the ABL at the mountain front in the NCP was obtained to explore the spatial heterogeneity of the ABL structure and haze pollution distribution.

Unlike previous experimental studies on haze pollution in the NCP, the COATS experiment focused on the spatial structure of the ABL and the turbulent exchange of pollutants between ground and atmosphere in the mountain front area. The boundary layer profiling was conducted together with ground-based observations, and the particulate sounding system was used to measure the meteorological and environmental elements simultaneously in the ABL, avoiding the use of ground-based remote sensing equipment which may cause greater inversion errors. The observation periods covered winter and summer, and the study area was monitored with a "point-line-surface" experiment layout. During the experiment, more than 3000 sets of boundary layer profiles containing $PM_{2.5}$ concentration data were collected, and the profile data of long time series and high spatial-temporal resolution were obtained from multiple experimental stations, which makes up for the limitations of previous experiments in the aspects of observation methods and station distribution. This experiment provided valuable information for studying the ABL spatial structure in the NCP and the turbulent exchange of pollutants between ground and atmosphere.

2.1 Single-station "point" experiments from 2016 to 2018

The observation periods, observed variables, and instruments used in the "point" experiments from 2016 to 2018 are summarized in Table 1. In 2016, intensified observations on the ABL in winter and summer were carried out at Cangzhou station. Cangzhou station is located in a suburban area with a flat and uniform underlying surface. Intensive sounding observation was carried out eight times a day at 02:00, 05:00, 08:00, 11:00, 14:00, 17:00, 20:00 and 23:00 (UTC/GMT + 08:00), respectively, using the XHD-403 sounding balloon produced by the Institute of Atmospheric Physics, Chinese Academy of Sciences. The data were recorded every second to generate the temperature, relative humidity, wind speed, and wind direction profiles, and 160 sets of sounding records were collected in the winter and summer of 2016, respectively. Meanwhile, the 100-m-high meteorological tower at the experimental station was installed with ultrasonic anemometer-thermometers at 30 m and 100 m heights to monitor fluctuations of wind velocity and temperature to study turbulent diffusion features of pollutants.

From 2017 to 2018, three phases of intensive ABL experiments were conducted at Dezhou station. Dezhou station is located in Pingyuan County, Dezhou City, Shandong Province, in the central part of the NCP. There is flat and uniform farmland as the underlying surface, and the local meteorological features and air quality conditions are highly representative for the NCP. Sounding observations were conducted every three hours during these three phases of experiments. The sounding system used in winter 2017 and summer 2018 was the same as that used in the 2016 experiment in Cangzhou. The new particulate sounding system with a particulate concentration sensor (XHD-403/PMS5003T sounding balloon) developed by the Institute of Atmospheric Physics, Chinese Academy of Sciences, was first applied in the winter of 2018. With a portable particulate sensor added to the original sounding balloon, the mass concentrations of particulate matter (PM_{10}, $PM_{2.5}$, and PM_1) can be detected directly, and high-resolution simultaneous measurements of meteorological and environmental elements are realized, providing essential data for studying the

Table 1 Information of "point" observation experiments from 2016 to 2018

Station	Observation period	Observed variables	Instrument
Cangzhou 10 m, 38°17′N, 116°50′E	January 8, 2016, to January 28, 2016 May 27, 2016, to June 16, 2016	Wind, temperature, and humidity profiles	XHD-403 sounding balloon
		Atmospheric turbulence (wind and temperature) 30 m/100 m	CSAT3, Campbell, USA
Dezhou 24 m, 37°09′N, 116°26′E	December 25, 2017, to January 24, 2018 (Ground-based observations started on January 12, 2018)	Wind, temperature, and humidity profiles	XHD-403 sounding balloon
		Atmospheric turbulence (wind, temperature, humidity, and CO_2)	IRGASON, Campbell, USA
		Radiation	NR-Lite, Kipp & Zonen, the Netherlands
		Barometric pressure	CS106, Campbell, USA
	May 15, 2018, to June 14, 2018	Wind, temperature, and humidity profiles	XHD-403 sounding balloon
		Atmospheric turbulence (wind, temperature, humidity, and CO_2)	IRGASON, Campbell, USA
		Radiation	NR-Lite, Kipp & Zonen, the Netherlands
		Barometric pressure	CS106, Campbell, USA
	December 28, 2018, to January 24, 2019	Wind, temperature, humidity, and PM profiles	XHD-403/PMS5003T sounding balloon
		Atmospheric turbulence (wind, temperature, humidity, and CO_2)	IRGASON, Campbell, USA
		Radiation	NR-Lite, Kipp & Zonen, the Netherlands
		PM mass concentrations	E-Sampler, Met One, USA
		Visibility	CS120A, Campbell, USA
		Barometric pressure	CS106, Campbell, USA

characteristics of the ABL structure during haze pollution and the influencing mechanisms on pollution. The particulate sounding system achieved desirable performance in monitoring meteorological elements and particulate matter concentrations in the ABL. The same sounding system was used in the subsequent "line" profiling experiment and "surface" networking experiment for intensive sounding observations, and the operation specifications followed during the observations were the same. An integrated ultrasonic anemometer-thermometer and water vapor/CO_2 analyzer, modified scattering-type visibility meter, net radiometer, and particulate matter sampler were equipped at Dezhou station to monitor the atmospheric turbulence, visibility, radiation, particulate matter concentrations, and conventional meteorological elements in the surface layer. The specific instrument types and configurations are shown in Table 1.

2.2 "Line" profiling experiment in summer 2019

From June 17, 2019, to July 6, 2019, a "line" profiling experiment was carried out at Tuonan, Baoding, and Renqiu stations, which are distributed on a straight line perpendicular to the trend of the Taihang Mountains in the mountain front area of the NCP. These experimental stations are all in suburban regions, of which Tuonan station is the closet to the mountainous area, with a relatively high elevation of 190 m, while Baoding and Renqiu stations sit are at low elevations of roughly 20 m and 10 m, respectively. Intensive sounding observations, including particulate matter concentration measurements, were carried out at these experimental stations. Simultaneous ground-based observations on barometric pressure, atmospheric turbulence, radiation, and particulate matter concentrations were conducted at Tuonan and Renqiu stations. The observed variables and instruments used at each experimental station are summarized in Table 2.

2.3 "Surface" networking experiment in winter 2019

From November 26, 2019, to December 26, 2019, a "surface" networking experiment was conducted in the mountain front area of the NCP, with Bazhou, Baoding, and Dingzhou stations distributed from north to south along the trend of the Taihang Mountains and Tuonan, Baoding, Renqiu, and Cangzhou stations distributed from west to east on a straight line perpendicular to the Taihang Mountains. The layout of these stations forms a cross-shaped observation network centered at Baoding. Dingzhou station is close to the mountainous area, with an elevation of about 60 m, while Bazhou and Cangzhou stations are at elevations of approximately 10 m. Intensive sounding observations were carried out at all six stations simultaneously, while atmospheric turbulence, visibility, particulate matter concentrations, radiation, and barometric pressure data in the surface layer were monitored at Tuonan, Baoding, and Renqiu stations. The observed variables and instruments used at each experimental station are summarized in Table 3.

Table 2 Information of the "line" profiling experiment in summer 2019

Station	Observed variables	Instrument
Tuonan 188 m, 39°1′N, 115°7′E	Wind, temperature, humidity, and PM profiles	XHD-403/PMS5003T sounding balloon
	Barometric pressure	CS106, Campbell, USA
	Atmospheric turbulence (wind and temperature)	CSAT3, Campbell, USA
	Radiation	NR-Lite, Kipp & Zonen, the Netherlands
Baoding 19 m, 38°47′N, 115°30′E	Wind, temperature, humidity, and PM profiles	XHD-403/PMS5003T sounding balloon
	Barometric pressure	CS106, Campbell, USA
Renqiu 10 m, 38°44′N, 116°6′E	Wind, temperature, humidity, and PM profiles	XHD-403/PMS5003T sounding balloon
	Barometric pressure	CS106, Campbell, USA
	Atmospheric turbulence (wind, temperature, humidity, and CO_2)	IRGASON, Campbell, USA
	Radiation	LI200X, LI-COR, USA
	Visibility	CS120A, Campbell, USA

Table 3 Information of the "surface" networking experiment in winter 2019

Station	Observed variables	Instrument
Tuonan 188 m, 39°1′N, 115°7′E	Wind, temperature, humidity, and PM profiles	XHD-403/PMS5003T sounding balloon
	Atmospheric turbulence (wind and temperature)	CSAT3, Campbell, USA
	Radiation	NR-Lite, Kipp & Zonen, the Netherlands
	Visibility	CS120A, Campbell, USA
	Barometric pressure	CS106, Campbell, USA
Baoding 19 m, 38°47′N,115°30′E	Wind, temperature, humidity, and PM profiles	XHD-403/PMS5003T sounding balloon
	Atmospheric turbulence (wind, temperature, humidity, and CO_2)	IRGASON, Campbell, USA
	Radiation	CMP3, Kipp & Zonen, the Netherlands
	Visibility	CS120A, Campbell, USA
	Barometric pressure	CS106, Campbell, USA
Renqiu 10 m, 38°44′N, 116°6′E	Wind, temperature, humidity, and PM profiles	XHD-403/PMS5003T sounding balloon
	Atmospheric turbulence (wind, temperature, humidity, and CO_2)	IRGASON, Campbell, USA
	Radiation	LI200X, LI-COR, USA
	Visibility	CS120A, Campbell, USA
	Barometric pressure	CS106, Campbell, USA
Cangzhou 10 m, 38°17′N,116°50′E	Wind, temperature, humidity, and PM profiles	XHD-403/PMS5003T sounding balloon
	Barometric pressure	CS106, Campbell, USA
Dingzhou 56 m, 38°34′N, 115°0′E	Wind, temperature, humidity, and PM profiles	XHD-403/PMS5003T sounding balloon
	Barometric pressure	CS106, Campbell, USA
Bazhou 9 m, 39°8′N, 116°26′E	Wind, temperature, humidity, and PM profiles	XHD-403/PMS5003T sounding balloon
	Barometric pressure	CS106, Campbell, USA

3. Characteristics of the ABL and distribution of $PM_{2.5}$ concentrations in the NCP

3.1 Basic characteristics of the ABL

Mean diurnal variations of the potential temperature profiles in summer and winter at Dezhou station from 2017 to 2018 are plotted in Figure 2. The thermal structure indicated that the diurnal variation of the ABL was more pronounced in summer than in winter. In summer, a convective boundary layer (CBL) developed at 08:00 in the morning, and the boundary layer height reached an average of 1200 m at 17:00. A stable boundary layer (SBL) existed from 20:00 to 05:00 the next day, with a maximum height of about 350 m on average. In winter, a prominent CBL structure appeared at 11:00 and 14:00, and its maximum height was roughly 600 m on average. SBL existed from 17:00 to 08:00 the next day, with a maximum height of about 400 m. The dynamic structure (figure omitted) showed that the wind speed in

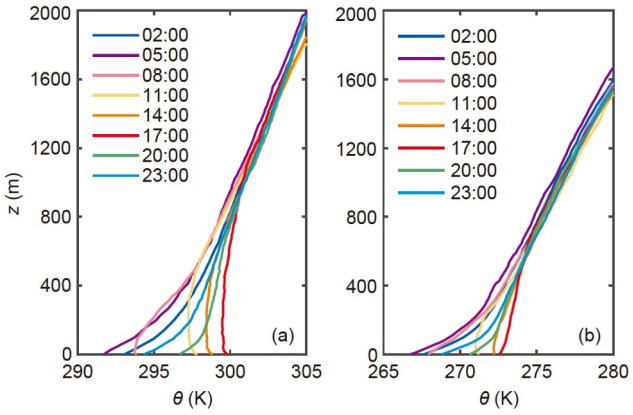

Figure 2 Mean diurnal variations of the potential temperature in summer (a) and winter (b) at Dezhou station from 2017 to 2018.

lower atmosphere was relatively low during daytime in winter and summer, and increased during nighttime, which means that low-level jets (LLJs) frequently occur in the NCP. The average wind speed in lower atmosphere was higher in summer than in winter, indicating that the horizontal transport capacity for substance and energy was also higher in summer. The humidity of the lower atmosphere also exhibited significant diurnal variations in winter and summer (figure omitted), with lower specific humidity during daytime and increased values during nighttime. The moisture conditions in the lower atmosphere were better in summer, with specific humidity ranging from 8 to 10 g kg^{-1}. In comparison, the entire atmosphere was dryer in winter, with an average specific humidity of about 1 g kg^{-1}. The specific humidity usually decreased monotonically with height in summer, while humidity inversion commonly occurred below 400 m in winter.

3.2 Characteristics of the distribution of $PM_{2.5}$ concentrations in the ABL

The evolution trends of haze pollution processes in the NCP have a certain consistency, for $PM_{2.5}$ usually accumulates slowly and is removed rapidly (Zhong et al., 2017; Li et al., 2020). In the accumulation stage of pollutants, the NCP tends to be controlled by a persistent low-pressure system characterized by stable barometric pressure field, low pressure gradient, and stagnant surface airflow. Such stagnant weather has also been noted by previous researchers (Yang et al., 2015; Ye et al., 2016; Kanawade et al., 2020). In the rapid dissipation stage of pollutants, the pressure gradient in the NCP increases, and the cold high-pressure system invades rapidly, accompanied by intense downward airflows. Figure 3 shows the spatial-temporal evolution of $PM_{2.5}$ concentrations and ABL structure at each experimental station during a typical haze pollution process monitored by the "surface" networking experiment in winter 2019. For the same haze pollution process, the variation of the vertical distribution of $PM_{2.5}$ concentrations and ABL structure at each experimental station was similar. However, the degree of pollution and the boundary layer meteorological conditions among these regions showed significant spatial differences. Overall, the pollution at Baoding was the heaviest, followed by that at Renqiu, and the pollution at Tuonan was the mildest. During the intensive experiment, about 70% of the observations at Tuonan were under clean weather conditions, whereas Baoding was troubled by frequent heavy pollution, with only 30% of observations under clean weather conditions. Such results are not only caused by pollution source emissions but also related to local meteorological conditions. The comparison of surface wind speed shows that the conditions with wind speed below 1 m s^{-1} accounted for 71%, 66%, and 55% of the observation period at Tuonan, Baoding, and Renqiu, respectively. The wind field at Tuonan was dominated by calm winds, while the wind speed at Renqiu was typically high. The proportion of the experimental period with temperature below 0°C accounted for 71%, 46%, and 18% at Tuonan, Baoding, and Renqiu, respectively, meaning that the temperature of the underlying surface was the lowest at Tuonan and highest at Renqiu. The surface wind speed and temperature exhibited an increasing trend from the mountainous regions in the west to the plain area in the east, which is associated with the blocking effect of mountains and drainage flow (Whiteman et al., 1999; Silcox et al., 2011).

In terms of the frequency of haze pollution events and the degree of pollution in winter and summer, during the observation period in summer, the number of days with clean weather exceeded 80%, and the overall degree of pollution was mild. Among the pollution events, mild pollution conditions accounted for 78% of all pollution periods. While in winter, haze pollution events accounted for about 50% of the entire observation period, and moderate to heavy pollution accounted for 60% of all pollution periods. For the spatial heterogeneity of haze pollution, as atmospheric circulations are more active in summer, which is conducive to the regional transport of pollutants, the spatial distribution of pollutants is more uniform in summer; in winter, stagnant weather conditions prevail, and pollutant concentrations are more strongly affected by local emissions and boundary layer meteorology, resulting in more pronounced spatial differences of winter haze pollution.

Based on the "line" profiling experiment in summer 2019 and "surface" networking experiment in winter 2019, the mean $PM_{2.5}$ column content during haze pollution in winter and summer was calculated for each experimental station. Different from the general belief, the $PM_{2.5}$ column content was higher in summer than in winter, indicating that the total $PM_{2.5}$ concentrations in the atmosphere may be higher in summer than in winter. This may be due to the higher hu-

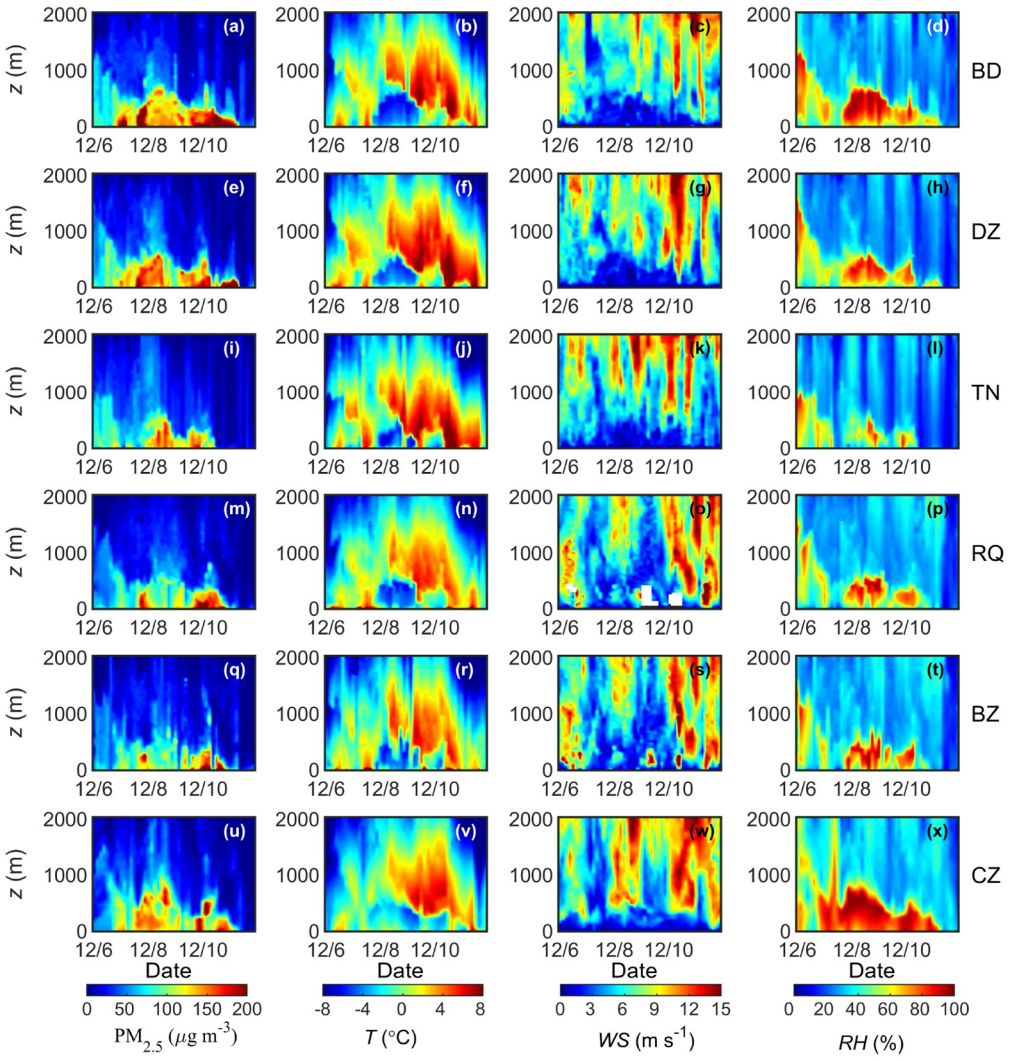

Figure 3 Spatial-temporal evolution of $PM_{2.5}$ concentrations and ABL structure at Baoding ((a)–(d)), Dingzhou ((e)–(h)), Tuonan ((i)–(l)), Renqiu ((m)–(p)), Bazhou ((q)–(t)), and Cangzhou ((u)–(x)) station during a typical haze pollution process monitored by the "surface" networking experiment in winter 2019 (Li, 2022).

midity and stronger atmospheric oxidation in summer, which are conducive to aerosol hygroscopic growth and aging and secondary aerosol generation (Ran et al., 2011; Zhang et al., 2015; Han et al., 2016; Wu et al., 2018; Pan et al., 2019). In addition, these results reflect the differences in the vertical distribution pattern of $PM_{2.5}$ in winter and summer. The "line" profiles of mean $PM_{2.5}$ concentrations at Tuonan, Baoding, and Renqiu stations during persistent haze pollution in winter and summer are shown in Figure 4. It can be seen that the mean $PM_{2.5}$ concentrations can exceed 150 μg m^{-3} during pollution periods in winter, but the aerosol-enriched layer is thin, and the diffusion height of $PM_{2.5}$ is only 400–500 m. The whole atmosphere was only mildly polluted in summer, with a $PM_{2.5}$ concentration typically below 100 μg m^{-3}. However, the pollution layer was thicker, $PM_{2.5}$ diffused to a height of nearly 1000 m and was uniformly dispersed. Thus, the accumulated $PM_{2.5}$ in the column can be higher in summer than in winter.

4. ABL three-dimensional structure and its contribution to $PM_{2.5}$ distribution

4.1 Influencing mechanisms of the ABL structure on the vertical distribution of $PM_{2.5}$

The structure of the ABL affects the horizontal transport, turbulent mixing, and chemical transformations of pollutants during haze pollution, directly or indirectly determining the vertical distribution and concentration variations of pollutants. Studying the ABL structure during heavy haze pollution is of great significance for understanding the generation, development, and dissipation processes of heavy haze pollution in the NCP. Here, the thermal, dynamic, and moisture structures of the ABL during heavy haze pollution in the NCP and their effects on the vertical distribution of $PM_{2.5}$ are thoroughly analyzed based on the sounding data.

Li Q H et al. (2020, 2021) discovered that during heavy haze pollution, the thermal structure of the ABL is often

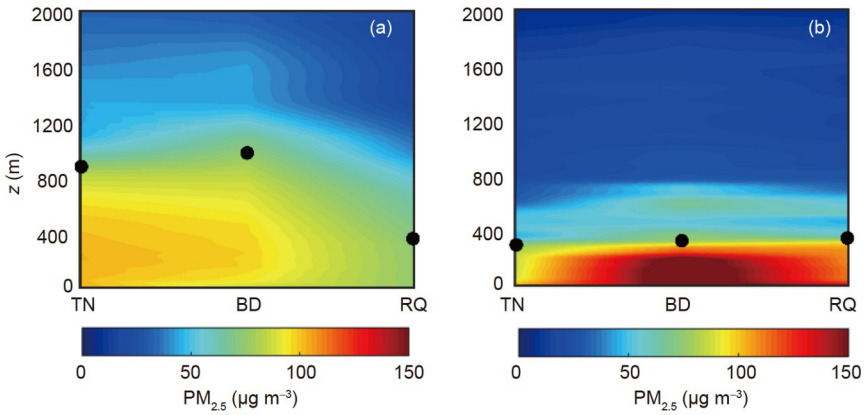

Figure 4 Profiles of mean $PM_{2.5}$ concentrations under haze conditions in summer (a) and winter (b) of 2019. Black dots show the thickness of pollution layer (Li, 2022).

characterized by an elevated inversion layer (EIL) that lasts for more than three days at low altitudes, and that the bottom height of this layer continuously decreases. The distribution of $PM_{2.5}$ concentrations and the thermal structure during a typical heavy haze pollution process are shown in Figure 5. With Dezhou station as an example, Figure 5b reveals that an EIL persisted at low altitudes from January 12 to 15, 2019, and the bottom height of this layer gradually decreased from 800 m to 200 m. The strong inversion layer with a thickness of about 200 m lasted for almost a whole day on January 14. Similar thermal structures were observed at the six experimental stations during the networking experiment in the NCP in the winter of 2019 (Figure 3). The patterns at Baoding station are illustrated in Figure 5c and 5d. Similar to the phenomenon observed at Dezhou station, a relatively prominent EIL persisted at low altitudes from December 8 to 10, 2019, and the bottom height of the inversion layer gradually decreased. Correspondingly, the thickness of the pollution layer was compressed from 800 m to about 200 m. Because of the strong stable atmospheric stratification, the upper and lower parts of the lower atmosphere cannot be coupled by turbulent flows, making it difficult for pollutants in the low layers to pass through the stable air layers to diffuse upward. Meanwhile, the momentum transport from the upper to lower atmosphere is hindered, leading to the formation of a thin and static layer below the EIL that facilitates the accumulation of pollutants in the surface layer. As the bottom height of the EIL decreases, the space for pollutant diffusion is continuously compressed, which significantly exacerbates the degree of pollution. Therefore, the long-lasting and continuously sinking EIL at low altitudes is the typical thermal structure responsible for persistent and exacerbated haze pollution.

The formation of the continuously sinking EIL is associated with the subsidence warming caused by the gusty cold-air invasion. For instance, from December 8 to 10, 2019, there was a stable trough at low altitudes over the NCP when the bottom height of the EIL was decreasing. With the invasion of cold air from the west, the trough was gradually deepened, downdrafts systematically developed in the cold advection zone behind the trough, and the intensity of the downward motion increased. The upper atmosphere was heated due to adiabatic warming generated by the downdrafts, leading to the maintenance of the EIL and decrease in its bottom height. Figure 6 shows the spatial patterns of the vertical velocity ω in the NCP at 08:00 from December 8 to 10, 2019, with positive values of ω indicating the downward motion. It can be seen that the downdrafts gradually enhanced from December 8 to 10, especially in the western areas close to the Taihang Mountains, which confirms that the thermal structure is related to subsidence warming.

For the dynamic structure, there are usually strong southerly winds within the boundary layer that promote the adjective transport of pollutants and moisture in the transport stage of pollutants, making the pollution layer relatively thick and the degree of pollution mild in the early stage. In the accumulation stage of pollutants, airflows are usually stagnant in the lower atmosphere, forming a calm wind layer with wind speed below 2 m s^{-1}, which is conducive to the accumulation of pollutants in the surface layer. During the rapid dissipation stage of pollution, LLJs occur frequently and develop from higher to lower altitudes. LLJs not only enhance the horizontal transport of pollutants but also generate mechanical turbulence through wind shear, promoting the momentum exchange between the upper and lower atmosphere and improving the vertical diffusion conditions (Banta et al., 2002; Wei et al., 2018, 2020; Li et al., 2020). As shown in Figure 7, the maximum wind speed of the LLJ increased from 7 to 13 m s^{-1} from 11:00 to 23:00 on December 19, 2018, and the height of the jet axis decreased from about 400 m to 200 m. As LLJs develop from higher to lower altitudes, turbulent flows are generated from the higher altitudes and transmitted downward, restoring the turbulent coupling between the upper and lower atmosphere from high altitudes downward, and the momentum at high altitudes transmits to the lower atmosphere. At the same time, $PM_{2.5}$ is cleared from higher to lower altitudes. Therefore, LLJs is one

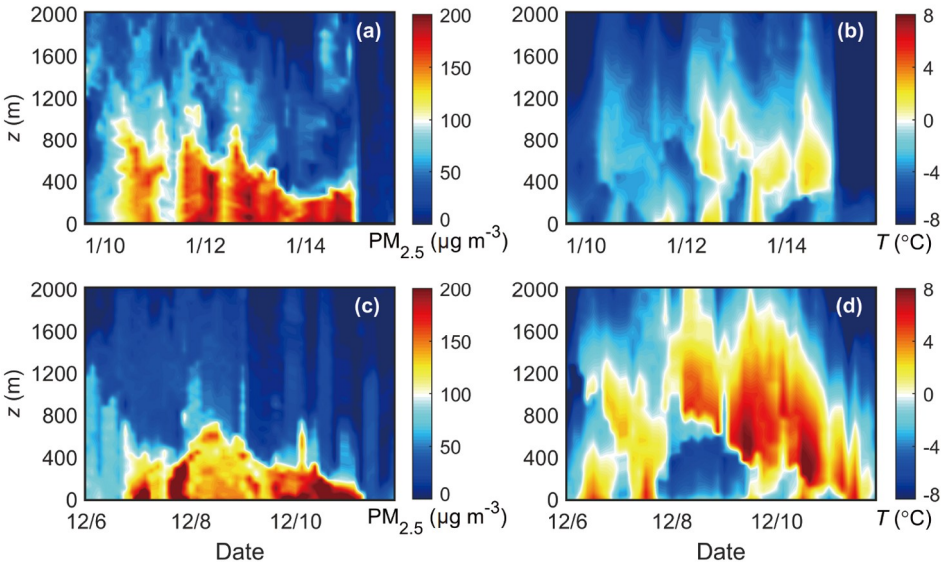

Figure 5 Vertical distribution of $PM_{2.5}$ concentrations and the thermal structure during a typical heavy haze pollution process. ((a)–(b)) Dezhou station, from January 10 to 15, 2019; ((c)–(d)) Baoding station, from December 6 to 11, 2019.

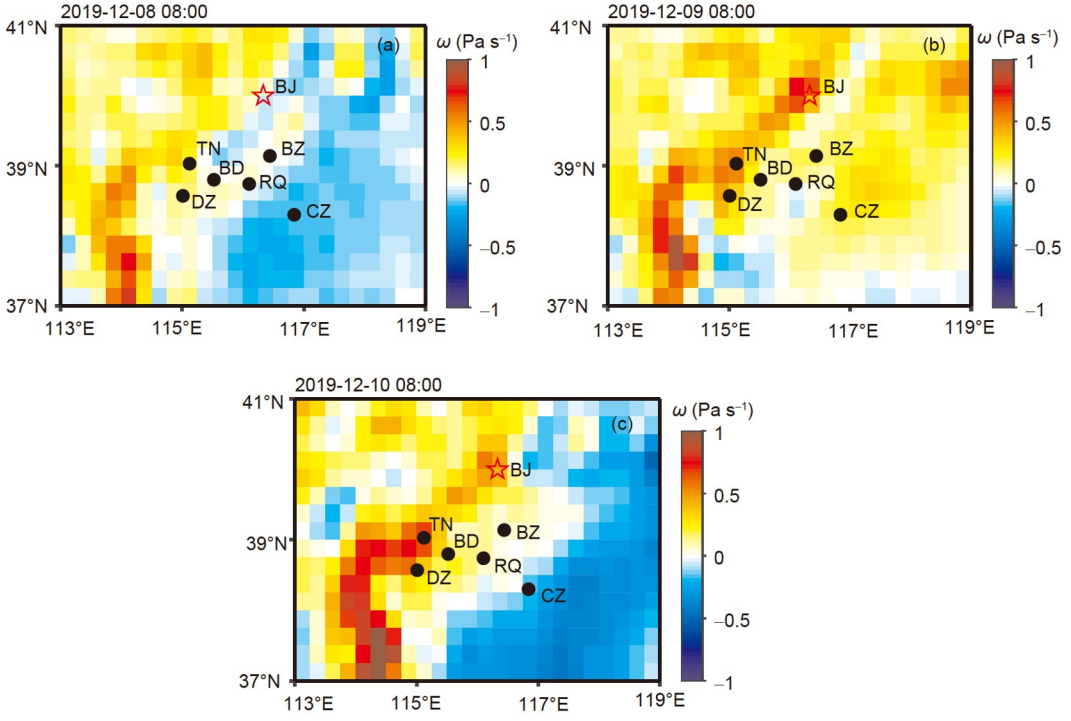

Figure 6 Vertical velocity ω at 925 hPa at 08:00 on December 8 (a), December 9 (b), and December 10 (c), 2019 (Li Q H et al., 2021, Open Access).

of the key physical mechanisms facilitating haze dissipation.

In terms of the moisture structure, under the influence of moisture transport by southerly winds and local accumulation, the relative humidity is typically high during persistent heavy haze pollution in the NCP. The region with the highest $PM_{2.5}$ concentrations often coincides with a wet zone with relative humidity above 60%. The high relative humidity is conducive to aerosol hygroscopic growth and secondary aerosol generation, which can easily cause heavy pollution. However, if the ambient air is almost saturated, aerosol particles may serve as condensation nuclei to form droplets, resulting in the decrease in $PM_{2.5}$ concentrations due to wet removal.

4.2 Influencing mechanisms of the ABL three-dimensional structure on regional pollution

The Taihang Mountains have an adjusting effect on the meteorological conditions of the ABL in the NCP, providing

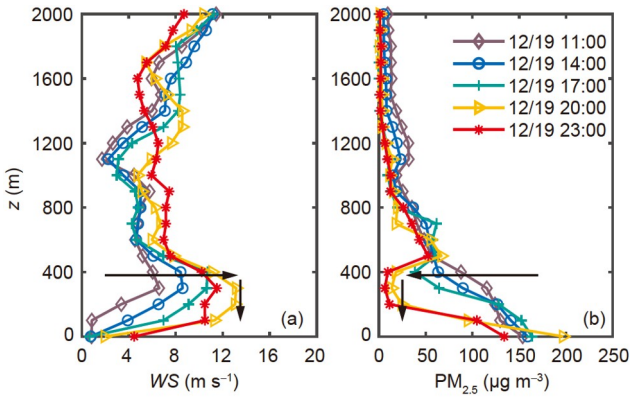

Figure 7 Evolution of wind speed (a) and $PM_{2.5}$ concentrations (b) profiles during the dissipation stage of pollution on December 19, 2018 (Li et al., 2020, Open Access).

the NCP with a spatially heterogeneous ABL and complex local circulations, which affects the spatial-temporal distribution of pollutants concentrations during haze pollution. The influencing mechanisms of the ABL three-dimensional structure and local circulations in the NCP on the spatial distribution of haze pollution were explored based on the data of "line" profiling and "surface" networking experiments and numerical simulation results (Li Q H et al., 2021; Jin et al., 2022a, 2022b).

Figure 8 demonstrates the three-dimensional structure of the ABL and the distribution of $PM_{2.5}$ concentrations during a typical haze pollution process in winter 2019. It can be seen that, due to the presence of the Taihang Mountains, there are significant differences in the ABL structure and the spatial distribution of $PM_{2.5}$ among different regions of the NCP. Comparing the surface pollution degree and meteorological elements at different experimental stations reveals that $PM_{2.5}$ concentrations and water vapor content were the highest at Baoding and lowest at Tuonan, which should be related to the locally high emission of pollutants at Baoding. Both temperature and wind speed values are the lowest at Tuonan station and the highest at Renqiu station due to the thermal and dynamic adjustment of the boundary layer meteorological conditions by the Taihang Mountains. In terms of thermal structure, the western part of the NCP near the mountains is significantly affected by drainage flow and subsidence warming, resulting in lower surface temperature, stronger EIL, more stable atmospheric stratification, and worse conditions for vertical diffusion of pollutants. For the dynamic structure, the mountainous terrain has a dynamic adjustment effect on the wind field. The blocking effect of mountains causes frictional loss of kinetic energy and leads to airflow diversion, weakening the ambient wind. As a consequence, the calm wind layer in the western part of the NCP near the mountains is relatively thicker, which is not conducive to the horizontal transport of pollutants. Therefore, the concentration of $PM_{2.5}$ is higher in the western area near the mountains and low in the eastern area over the plain.

Atmospheric pollutants usually come from anthropogenic emissions near the ground and disperse to higher altitudes through turbulent motions. Therefore, the pollutant concentrations usually decrease with height. However, during the COATS experiment, the phenomenon of elevated pollution layer (EPL) was observed, i.e., the pollutant concentrations were relatively low in the lower atmosphere but high at an altitude of 1000–2000 m. Figure 9 shows the vertical distribution of $PM_{2.5}$ concentrations during haze pollution in the NCP in summer 2019. We can see that during the rapid dissipation stage of pollutants, the $PM_{2.5}$ at low and high altitudes was not cleared simultaneously. $PM_{2.5}$ concentrations at the ground level decreased at 14:00 on June 21, but $PM_{2.5}$ concentrations abnormally increased in the altitude range of 1500–2000 m, showing an EPL (the red box in Figure 9). Li et al. (2022) analyzed the local circulation pattern and concluded that the formation of EPL is associated with mountain-induced vertical circulations. The wind fields at 1000 hPa and 800 hPa in the NCP at 14:00 and 20:00 on June 21, 2019, are plotted in Figure 10. When the NCP is located in the southern part of high-pressure system, the polluted air mass moves from the eastern plain area to the western mountainous regions under the advection of the easterly winds, and pollution outbreaks sequentially from Renqiu to Tuonan. Obstructed by the Taihang Mountains, the dynamic structure of the wind field is adjusted, and vertical circulations are induced, forcing the ground-level pollutants to rise with the easterly winds. According to Figure 10c and 10d, the wind direction clearly shifts at 800 hPa, so the surface pollutants lifted to high altitudes are transported back to the NCP by westerly winds, forming an EPL. Therefore, when studying the haze pollution at the mountain front areas of the NCP, we should not only focus on the accumulation of pollutants in the surface layer, but also consider the influence of EPLs generated by vertical circulations.

Jin et al. (2022a, 2022b) analyzed the ground-based observations of haze pollution in the NCP from 2014 to 2020 and classified three types of pollution according to the atmospheric internal boundary (AIB) conditions that triggered haze pollution, i.e., the frontal type, wind shear type, and topographic obstruction type. The proportions of these three types of pollution were roughly 41%, 29%, and 14%, respectively. The AIB conditions of the three types of pollution were explored by numerical simulations to clarify the ABL structure and elucidate the formation mechanism of the polluted air masses with distinct boundaries. Schematic diagrams of the AIBs of the three pollution types are illustrated in Figure 11. As shown in Figure 11a, frontal-type pollution arises under the mountain thermal effects and the warm front. The cold polluted air mass at the mountain front is covered by a dome-like warm cap, which restricted the diffusion of polluted air both in horizontal and vertical di-

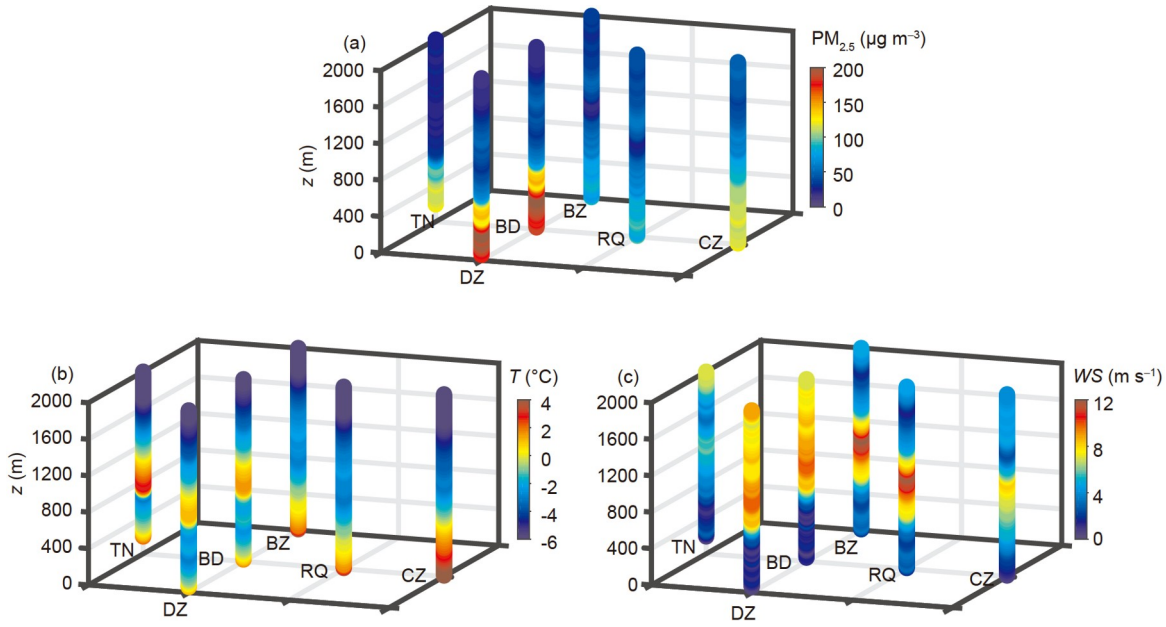

Figure 8 Three-dimensional structure of the ABL and distribution of $PM_{2.5}$ concentrations during a typical haze pollution process in winter 2019. (a) $PM_{2.5}$ concentrations; (b) temperature; (c) wind speed (Li Q H et al., 2021, Open Access).

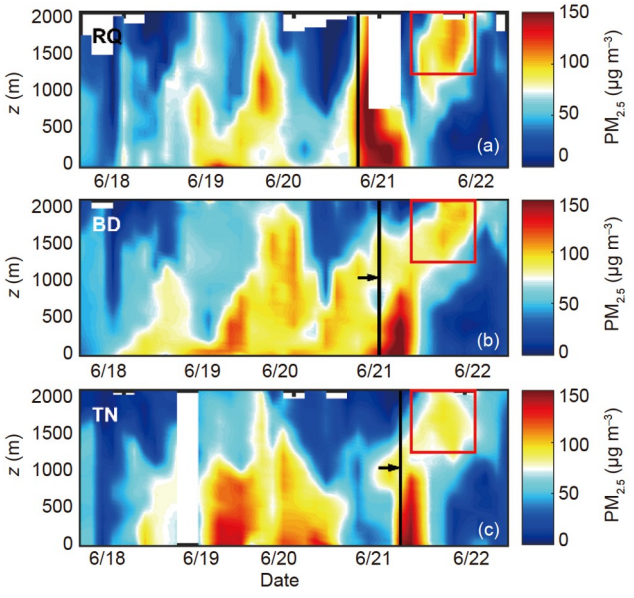

Figure 9 Vertical distribution of $PM_{2.5}$ concentrations at Renqiu (a), Baoding (b), and Tuonan (c) stations from June 18 to 22, 2019. The black line indicates the time of the pollution outbreak, the arrow suggests the time interval, and the red box delineates the EPL (Li, 2022).

rections. The ABLH in this region is only 200–300 m. Frontal-type pollution is usually severe as $PM_{2.5}$ accumulates rapidly in the near-closed space with stable atmospheric stratification (Jin et al., 2021). Wind shear type pollution is characterized by airflow convergence, mainly in two modes, the westerly-southwesterly wind shear and southerly-northerly wind shear, which provide dynamic conditions for pollutant transport and accumulation. This type of pollution is usually mild. Figure 11b shows the mode of westerly-southwesterly wind shear. It is characterized by a low-pressure trough, and the vertical scale of the airflow convergence layer is comparable to that of the ABL, with a divergence compensation layer above the boundary layer. The mode of southerly-northerly wind shear is characterized by a roughly 3000-m-thick, Y-shaped convergence layer opening to the west, and the top of the boundary layer is the region with peak convergence velocity. Features of topographic obstruction type pollution are revealed in Figure 11c, i.e., the cold air mass is dammed at the windward side in front of the mountains; the warm southerly advection is obstructed by the mountains and adjusted into cold easterly advection; air masses ascend after converging at the mountain front and then cool down, showing significant inversion at the boundary of the cold air zone. The dynamical feature is that there is an air mass convergence zone in front of the mountains. Diurnal variations of the ABL dynamic and thermal structures cause pollutants to accumulate in the foothills during the daytime and locally aggregate throughout the plain at nighttime.

4.3 Diffusion capacity of the ABL and its quantitative contribution to pollution in winter and summer

The situation of air pollution in the NCP is complicated, and persistent heavy haze pollution may occur in either winter or summer. Numerical simulations were performed using the data from "point" experiments at Dezhou station in winter 2018 to evaluate the relative contribution of different processes to $PM_{2.5}$ concentrations during haze pollution. The

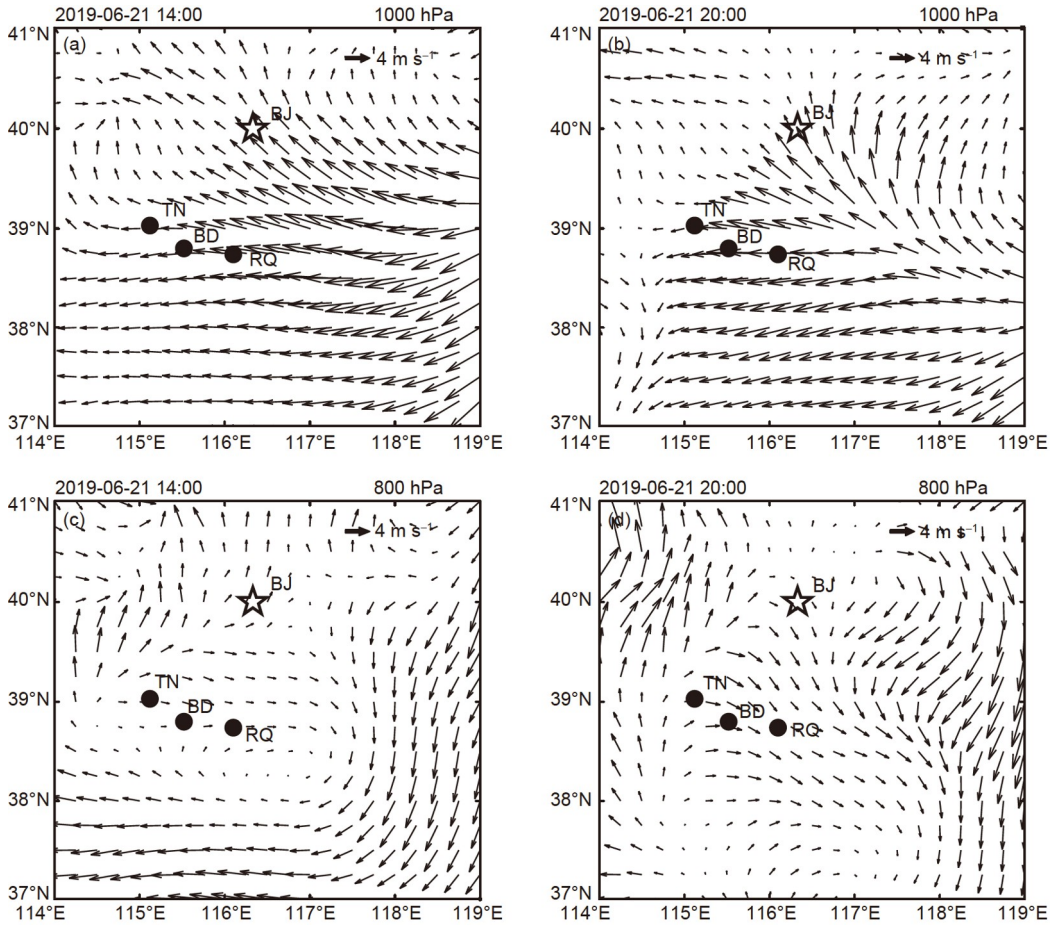

Figure 10 Wind fields at 1000 and 800 hPa in the NCP at 14:00 and 20:00 on June 21, 2019. (a) 14:00 at 1000 hPa; (b) 20:00 at 1000 hPa; (c) 14:00 at 800 hPa; (d) 20:00 at 800 hPa (Li et al., 2022, Open Access).

data of the "line" profiling experiment in summer 2019 and the "surface" networking experiment in winter 2019 were used to compare the vertical distribution of $PM_{2.5}$ concentrations and the diffusion capacity of the ABL in different seasons and quantitatively estimate the contribution of different scales of atmospheric motions to haze pollution in winter and summer.

Figure 12 shows the mean $PM_{2.5}$ concentrations, potential temperature, and wind speed profiles for the fully developed ABL at 14:00 at Baoding station in the summer and winter of 2019, where the dashed and solid lines denote clean and polluted periods, respectively, and the red dots denote the ABLH. It can be seen that the $PM_{2.5}$ diffusion height reached approximately 1000 m in summer and the degree of pollution was generally mild. While the $PM_{2.5}$ diffusion height was only 300 m to 400 m and the degree of pollution degree was mainly moderate to heavy in winter. The mean ABLH, wind speed, and boundary layer ventilation values of summer haze pollution were about 1000 m, 4 m s^{-1}, and 4000 m^2 s^{-1}, respectively, which were close to the values during clean periods. In contrast, the diffusion conditions deteriorated significantly during the pollution periods in winter, with mean ABLH, wind speed, and boundary layer ventilation values of only 500 m, 2 m s^{-1}, and 1400 m^2 s^{-1}, which were 45%, 50%, and 60% lower than the values in clean periods, respectively (Li et al., 2022).

Jin et al. (2020) used a box model to simulate the relative contribution of different physical processes to $PM_{2.5}$ concentrations in the NCP. The research confirmed that local source emissions and regional transport of pollutants play a dominant role in the generation of heavy haze events, with contributions of about 27–45% and 46–76%, respectively. Boundary layer processes were also important regulators for $PM_{2.5}$ concentrations, such as temporary accumulation of $PM_{2.5}$ during the day-night transition periods and the variations of ABLH, which had contributions of about 13–40% and −6–22%, respectively. Li et al. (2022) applied spectral analysis method to surface $PM_{2.5}$ concentrations, and discovered weekly and diurnal variation cycles of $PM_{2.5}$ concentrations, which corresponded to the effects of weather systems and boundary layer processes, respectively (Figure 13). The contributions of weather system changes and boundary layer processes to $PM_{2.5}$ concentration in summer were about 45 and 15 μg m^{-3}, respectively, with a ratio of

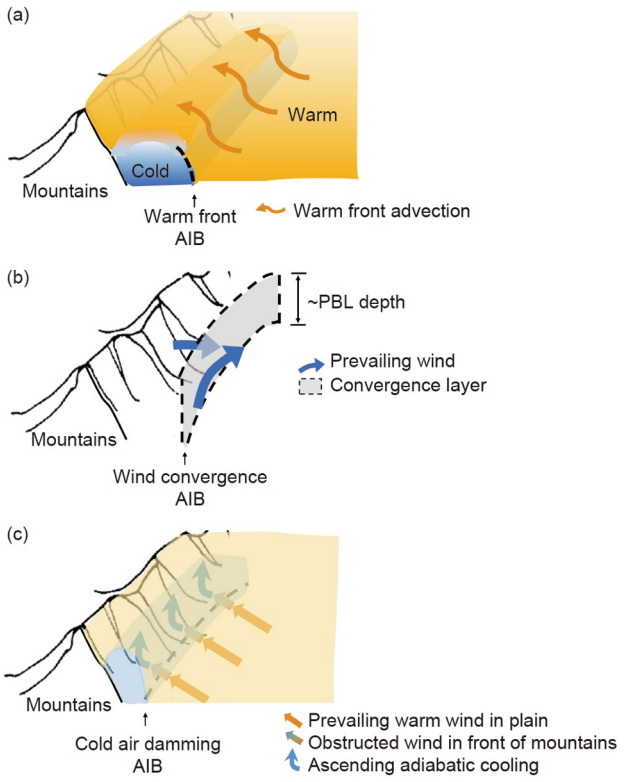

Figure 11 Schematic diagrams of the atmospheric internal boundaries (AIBs) of three pollution types in front of the Taihang Mountains. (a) Frontal type; (b) wind shear type; (c) topographic obstruction type (Jin et al., 2022a, Open Access).

nearly 3:1. In winter, the contributions were 40 and 30 μg m^{-3}, respectively, with a ratio of about 1.3:1. Weather systems can alter the regional circulation in the NCP and affect the regional transport of pollutants, thereby playing a key role in the generation of summertime haze pollution in the NCP. In winter, apart from the important contribution of the weather system to haze pollution events, the role of boundary layer processes is of equal significance and cannot be ignored.

5. ABLH and $PM_{2.5}$ distribution pattern

5.1 Relationship between surface $PM_{2.5}$ concentrations and the ABLH

According to Li et al. (2020), surface $PM_{2.5}$ concentrations are negatively correlated with CBL height and does not have an apparent correlation with SBL height. Figure 14 demonstrates the relationship between the ABLH and surface $PM_{2.5}$ concentrations based on the "point" experiment at Dezhou station in winter 2018. Due to the non-stationary nature of atmospheric motions during day-night transition periods, only the data at the time with relatively stationary atmospheric motions are used in this diagram. The observations at 11:00 and 14:00 correspond to a daytime CBL and those at 02:00 and 23:00 correspond to a nighttime SBL. It should be noted that high surface $PM_{2.5}$ concentrations may still occur even when the SBL height is high, which means that the influencing mechanisms of physical processes in the SBL on $PM_{2.5}$ concentrations are complex. The relationship between the ABLH and surface $PM_{2.5}$ concentrations is closely associated with turbulent transport capacity of the ABL, and

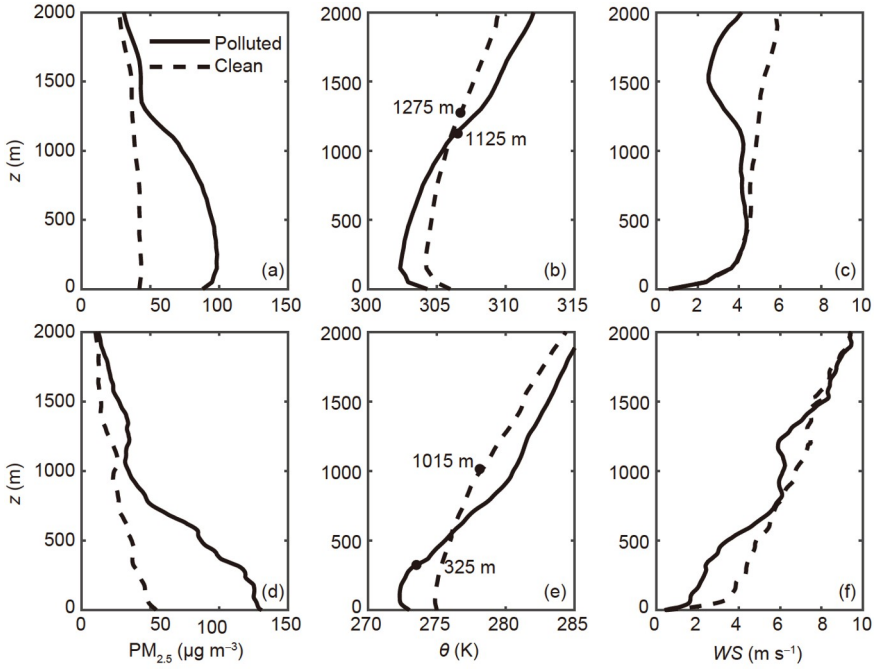

Figure 12 Mean $PM_{2.5}$ concentrations, potential temperature, and wind speed profiles at 14:00 at Baoding station in the summer ((a)–(c)) and winter ((d)–(f)) of 2019. Dashed lines: clean periods; solid lines: polluted periods; black dots: ABLH (Li et al., 2022, Open Access).

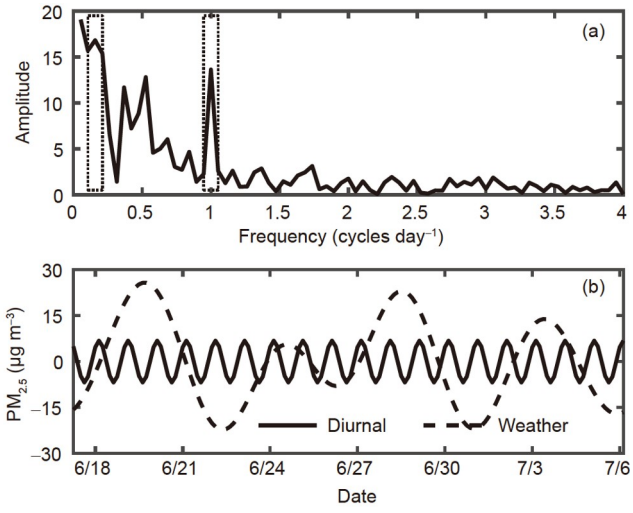

Figure 13 Spectral analysis of surface $PM_{2.5}$ concentrations at Baoding station in summer 2019. (a) Amplitude spectrum of $PM_{2.5}$ concentrations, with significant peaks delineated in the dashed boxes; (b) diurnal signals and weather signals (Li et al., 2022, Open Access).

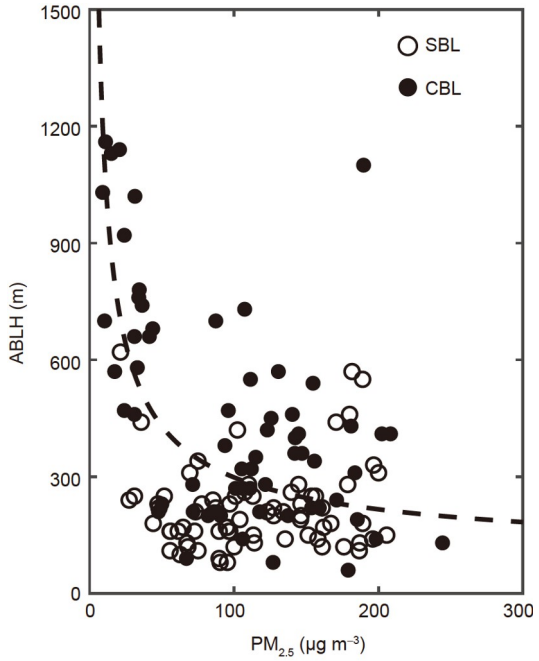

Figure 14 Relationship between the ABLH and surface $PM_{2.5}$ concentrations at Dezhou station in winter 2018 (Li et al., 2022, Open Access).

the turbulent motion of the SBL is intermittent (Ren et al., 2019b). The turbulent transport capacity was measured by the local intermittent strength of turbulence (LIST) index. The results showed that in the CBL and clean atmosphere, the turbulent transport capacity within the boundary layer was strong, but turbulence intermittency frequently occurred in the SBL and under heavy haze pollution conditions. It can be concluded that turbulence intermittency is an important factor influencing the relationship between the ABLH and surface $PM_{2.5}$ concentrations. If we regard the ABL as a box model, with strong turbulent mixing in the CBL and uniformly distributed pollutants, the relationship between the ABLH and $PM_{2.5}$ concentrations can be well established. The $PM_{2.5}$ concentrations within the SBL did not decrease with the increase of the SBL height, which may attribute to the prominent turbulent intermittency in the SBL. This study attempted to explain the effect of different types of turbulent intermittency on pollutant transport in the SBL. Intermittent turbulent bursts can facilitate the transport of pollutants from the residual layer into the SBL. When turbulent intermittency exists persistently during nighttime, turbulent transport may be spatially inhibited so that pollutants cannot be mixed uniformly within the boundary layer, making it difficult to establish a correlation between the SBL height and surface $PM_{2.5}$ concentrations.

5.2 Relationship between vertical distribution of $PM_{2.5}$ concentrations and the ABLH

Pollutants can serve as tracers to reflect atmospheric motions and structures (Collis et al., 1964; Collis and Ligda, 1964; Shi et al., 2019). Shi et al. (2020) named the atmospheric layer identified based on the vertical distribution of pollutants as the "material boundary layer". In the present study, this method for determining the ABLH was called the "material method". However, the pollutant diffusion height is often different from the traditional ABLH obtained based on meteorological elements. The physical meaning of the "material boundary layer" needs to be further clarified, and the reliability and applicability of the "material method" for ABLH inversion still need to be verified. In the COATS experiment, the physical concept "aerosol accumulation layer" (AAL) was proposed. According to the National Environmental Protection Standards of China, air is classified as polluted when $PM_{2.5}$ is the primary pollutant and its mass concentration exceeds 75 μg m^{-3}. Thus, the AAL was defined as the aerosol-enriched layer with $PM_{2.5}$ concentrations of over 75 μg m^{-3} above the ground. Figure 15a compares the AAL with the ABL and the results show that the spatial range of the AAL is consistent with that of the daytime CBL; however, the nighttime AAL tends to be higher than the SBL. Figure 15b further compares the height of the CBL with that of the AAL at 20:00 on the same day and good consistency is shown when the atmospheric motion is relatively stationary. It is conceivable that the vertical distribution of $PM_{2.5}$ in the daytime mainly depends on thermodynamic turbulent mixing, and the daytime distribution pattern of $PM_{2.5}$ concentrations in the CBL is maintained at night, i.e., the AAL depth in the nighttime reflects the height of the top of the residual layer, which leads to a large difference between the AAL depth and SBL height at night. Previous studies have also found that the distribution of $PM_{2.5}$ at night is weakly dependent on the evolution of the SBL (Liu et al., 2020). As a

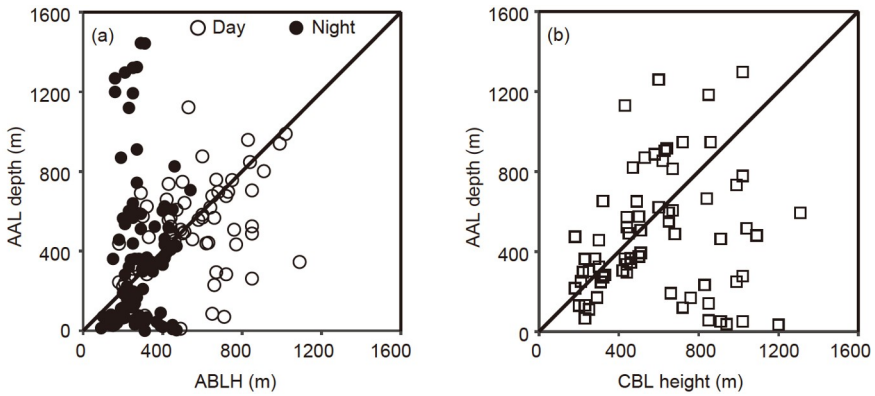

Figure 15 Comparisons of the ABLH with the AAL depth (a) and daytime CBL with the nighttime AAL (b) on the same day (Li et al., 2022, Open Access).

result, the inversion of the SBL height based on the vertical distribution of pollutants has poor accuracy (Wang et al., 2012; Lee et al., 2019). Therefore, the material method to determine the ABLH is applicable to the daytime CBL with stationary atmospheric motions and sufficient turbulent mixing. For the SBL at night, as well as the transport stage or rapid dissipation stage of pollutants with non-stationary atmospheric motions, determining the ABLH using the material method would cause significant deviations.

6. Turbulent flux acquisition and the turbulent characteristics of $PM_{2.5}$ concentrations

The ABL is a channel for the exchange of substance, including $PM_{2.5}$, between the ground and the atmosphere, with turbulent transport acting as the dominant form of exchange. Accurately acquiring the turbulent flux of $PM_{2.5}$ concentrations is an essential task in haze pollution studies, which is significant for the quantitative assessment of pollutant diffusion and deposition and the improvement of ABL parameterization schemes and the air quality forecasting.

Based on the theories of atmospheric turbulence and atmospheric optics, scholars at Peking University proposed a method to obtain the turbulent flux of $PM_{2.5}$ concentrations based on signal recognition and data processing techniques and developed the turbulent flux measurement system PMFlux (Ren et al., 2020). PMFlux consists of a three-dimensional ultrasonic anemometer-thermometer, a continuous particulate matter monitor, and a modified scattering-type visibility meter with high-frequency sampling performance that can provide 10 Hz wind velocity fluctuation, 1 Hz $PM_{2.5}$ mass concentrations, and 1 Hz visibility (extinction coefficient) data, respectively. The turbulent flux of $PM_{2.5}$ concentrations was calculated based on the eddy correlation method and theories of atmospheric optics. The specific calculation method was as follows. When the relative humidity is <80%, the extinction effect of $PM_{2.5}$ is considered to be the main reason for visibility reduction. The regression equation between the $PM_{2.5}$ concentrations and visibility (extinction coefficient) is established based on the observation results to determine the fitting coefficient for different pollution periods. The fluctuations of $PM_{2.5}$ concentrations are calculated using the high-frequency visibility (extinction coefficient) data, and the turbulent flux of $PM_{2.5}$ concentrations is obtained using the eddy correlation method with the wind velocity fluctuation data collected by the ultrasonic anemometer-thermometer. The operation procedures are simple, and the data processing technique is mature. This method can be applied together with the available turbulent flux measurement system or as a standalone observation system. It has performed well in the COATS experiment.

Based on the "point" experiment at Dezhou station in winter 2018 and "surface" networking experiment in winter 2019, the fluctuation and turbulent flux of $PM_{2.5}$ concentrations during the observation periods were obtained and the results exhibited the following characteristics. The turbulent flux of $PM_{2.5}$ concentrations varied in the range of –1–2 μg m^{-2} s^{-1} and the mean turbulent flux of $PM_{2.5}$ concentrations may be positive or negative in different haze processes and stages, indicating that the source-sink properties of the pollutant were not static. The absolute value of the turbulent flux of $PM_{2.5}$ concentrations decreased exponentially with the increase of turbulent kinetic energy, horizontal wind speed, wind speed standard deviation, momentum flux, and sensible heat flux. With enhanced turbulent diffusion capacity, $PM_{2.5}$ was mixed by strong turbulent motions and diffused away, and its turbulent flux value decreased. Moreover, the absolute turbulent flux value of $PM_{2.5}$ concentrations did not have a significant correlation with the $PM_{2.5}$ concentrations, possibly because turbulent motions tended to be weak during heavy haze pollution. Based on the observed turbulent flux of $PM_{2.5}$ concentrations, Ren et al. (2020) concluded that under unstable conditions, the relationship between the normalized standard deviation of $PM_{2.5}$ concentrations σ_c / C_*

and stability parameter ζ fulfills a 1/3 power law, with $\sigma_c / C_* = 20.07(-\zeta)^{-1/3}$; while the results under stable conditions were relatively discrete. The variance spectrum of the $PM_{2.5}$ concentration fluctuation ($nS_{PM_{2.5}}(n) / \sigma_c^2$) agrees with the Kolmogorov theory, with the spectral pattern in the inertial sub-region satisfying the 2/3 power law. The covariance spectrum of the $PM_{2.5}$ concentration fluctuation and vertical velocity fluctuation ($nC_{wPM_{2.5}}(n) / \sigma_w\sigma_c$) fulfills the –4/3 power law in the inertial sub-region. The above results show that the $PM_{2.5}$ concentration fluctuation follows the Monin-Obukhov similarity theory under certain conditions, and that the $PM_{2.5}$ concentration can be modelled by a universal function, like momentum or temperature. Figure 16 demonstrates the fitted universal functions of $PM_{2.5}$ concentrations $\varphi_c(\zeta)$ in relation to the stability parameter ζ at Dezhou station in winter 2018. Under unstable conditions, $\varphi_c(\zeta) = 4.0(1-9.8\zeta)^{-1/2}$ and under stable conditions, $\varphi_c(\zeta) = 4.0(1+1.2\zeta)^1$. Similarly, Ren et al. (2021) used data from the "surface" networking experiment in winter 2019 and determined that the results of different regions and different pollution processes varied: under unstable conditions, the universal functions for Tuonan, Baoding, and Renqiu were $\varphi_c(\zeta) = 1.5(1-3.5\zeta)^{-1/2}$, $\varphi_c(\zeta) = 2(1-12\zeta)^{-1/2}$, and $\varphi_c(\zeta) = 2.5(1-0.25\zeta)^{-1/2}$, respectively, compared to $\varphi_c(\zeta) = 1.5(1+1\zeta)^1$, $\varphi_c(\zeta) = 2(1+10\zeta)^1$, and $\varphi_c(\zeta) = 2.5(1+1\zeta)^1$ under stable conditions. The successful acquisition of the universal function for $PM_{2.5}$ concentrations provides an essential experimental basis for establishing the flux-profile relationship of $PM_{2.5}$ concentrations and parameterizing the turbulent flux of $PM_{2.5}$ concentrations.

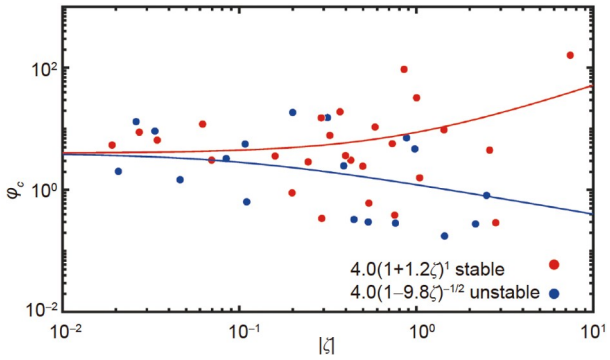

Figure 16 Relationships between the universal function of $PM_{2.5}$ concentrations $\varphi_c(\zeta)$ and the stability parameter ζ fitted with the data from Dezhou station in winter 2018. Red dots and blue dots denote stable and unstable conditions, respectively (Ren et al., 2020, Open Access).

7. Conclusions

From 2016 to 2020, Peking University, together with the Chinese Academy of Meteorological Sciences and the Institute of Atmospheric Physics, Chinese Academy of Sciences, carried out the COATS experiment in the NCP. Based on the "point" experiments, the basic characteristics of the ABL structure in the NCP were obtained and the influencing mechanisms of the ABL structure evolution on the vertical distribution of $PM_{2.5}$ was investigated. Through the "line" experiment, our understanding on the ABL processes and distribution of $PM_{2.5}$ concentrations during summer haze pollution was improved, and the contributions of the ABL processes to haze pollution in winter and summer were compared and estimated. The implementation of the "surface" experiment further enriched our understanding of the ABL three-dimensional structure and local circulation patterns in front of the Taihang Mountains, and the formation mechanism of the special spatial distribution pattern of haze pollution in the NCP was analyzed. The ABLH determines the vertical diffusion space of pollutants, which is a key parameter for air quality models to assess atmospheric diffusion conditions. Understanding the turbulent transport law of $PM_{2.5}$ is the basis for modifying the ABL parameterization schemes applicable to haze weather. Based on the data obtained in the COATS experiment, the indicative significance of the ABLH for air quality and the applicability of the material method to estimate the ABLH were thoroughly discussed. The turbulent transport characteristics of $PM_{2.5}$ were explored. The main findings are as follows:

(1) Basic characteristics of the ABL structure and $PM_{2.5}$ concentration distribution. The average CBL height in the NCP is about 1200 m in summer and 600 m in winter; the average SBL height is roughly 350 m in summer and 400 m in winter. In terms of the dynamic and moisture structures, LLJs frequently occur in the NCP, and humidity inversion is common in winter. Haze pollution in summer is predominantly mild, and the spatial distribution of pollutants is relatively uniform. In contrast, the pollution degree in winter is mostly moderate to heavy, with a significantly heterogeneous spatial distribution of pollutants. The $PM_{2.5}$ column content is higher in summer than in winter. The diffusion height of $PM_{2.5}$ in summer can reach 1000 m and mean $PM_{2.5}$ concentrations in the polluted layer is lower than 100 μg m^{-3}; the diffusion height of $PM_{2.5}$ in winter is only 400~500 m, with mean $PM_{2.5}$ concentrations of up to 150 μg m^{-3}.

(2) Influencing mechanisms of the ABL structure evolution on the vertical distribution of $PM_{2.5}$. The continuously sinking EIL which inhibits pollutant diffusion, hinders the downward momentum transfer, and compresses the diffusion space of pollutants, is a typical thermal structure promoting the maintenance and exacerbation of haze pollution. The formation of such a thermal structure is related to the subsidence warming caused by the gusty cold-air invasion. The mechanism of pollutant removal by LLJs was also revealed. LLJs

develop from higher to lower altitudes, promoting the generation of shear turbulence. The turbulent coupling between the upper and lower atmosphere is restored from high altitudes downward, and the momentum at high altitudes is transmitted to the lower atmosphere, facilitating the removal of pollutants from high altitudes downward. During heavy haze pollution, the region with the highest pollutant concentration often coincides with a wet zone with relative humidity above 60%. When the air is almost saturated with moisture, the pollutant concentration can be reduced by wet removal.

(3) Influencing mechanisms of the ABL three-dimensional structure and local circulations on the spatial distribution of haze pollution. Due to the adjustment of the thermal and dynamic structures of the ABL forced by the Taihang Mountains, the atmospheric stratification in the western part of the NCP is more stable, and the calm wind layer is relatively thicker, which facilitates local pollutant accumulation. As a consequence, haze pollution in the NCP is heavier in the west and milder in the east. The Taihang Mountains can induce vertical circulations, forcing ground-level pollutants to ascend with the easterly winds and be advected back over the plain at high altitudes, thereby forming the EPL. The internal boundary effect within the atmosphere restricts the horizontal diffusion of pollutants so that the polluted air masses are characterized by distinct boundaries. According to the internal boundary conditions, there are three main types of pollution: frontal type, wind shear type, and topographic obstruction type. The frontal type occurs when a cold air mass is jointly confined by the mountains and the internal boundary of the warm front, vertically covered by a dome-like warm cap. It is the most dominant type that triggers severe air pollution. The wind shear type is characterized by airflow convergence, mainly in two modes: westerly-southwesterly wind shear and southerly-northerly wind shear, which affects the spatial distribution of pollutants through dynamical effects. The topographic obstruction type is characterized by the accumulation of cold air in front of the mountains, and a heavy pollution zone is formed at the mountain front under the combined effect of dynamic blockage and thermal stratification.

(4) Comparative analysis and quantitative estimation of the contribution of the ABL processes to haze pollution in winter and summer. During the pollution periods in winter, the ABL diffusion conditions deteriorate significantly, with a decrease in the ABLH, wind speed, and boundary layer ventilation by 45%, 50%, and 60%, respectively. The contribution of the ABL processes to haze pollution in winter and summer was estimated using the spectral analysis method. The results showed that the regional transport of pollutants due to weather system changes has a critical contribution to haze pollution in summer, and for wintertime haze pollution, both weather system changes and boundary layer processes have significant contributions.

(5) ABLH and $PM_{2.5}$ distribution pattern. Surface $PM_{2.5}$ concentrations are found negatively correlated with the CBL height but has no apparent relationship with the SBL height. This is related to the strong turbulence intermittency of the SBL. Turbulent intermittency can spatially block the turbulent transport of pollutants so that the pollutants cannot be mixed within the boundary layer. Intermittent turbulent bursts can facilitate the transport of pollutants from the residual layer to the SBL. Both conditions may lead to box model failure. The concept of the AAL was proposed. It was found that the spatial range of the AAL is highly consistent with that of the CBL, but there is a large difference between the AAL and the SBL under the influence of the residual layer. The material method is applicable to the daytime CBL with stationary atmospheric motions and sufficient turbulent mixing. For the nighttime SBL and non-stationary atmospheric motion conditions, using the material method will cause large biases.

(6) Turbulent flux acquisition and turbulence characteristics of $PM_{2.5}$ concentrations. The method to obtain the $PM_{2.5}$ concentration turbulent flux based on the eddy correlation method and theories of atmospheric turbulence and atmospheric optics was proposed, and the turbulent flux measurement system PMFlux was developed. It was discovered that under unstable conditions, the normalized standard deviation of $PM_{2.5}$ concentration fluctuation σ_c / C_* and stability parameter ζ fulfills a 1/3 power law, which agrees with the Monin-Obukhov similarity theory. The variance spectrum of $PM_{2.5}$ concentration fluctuation $(nS_{\mathrm{PM}_{2.5}}(n) / \sigma_c{}^2)$ fulfills the $-2/3$ power law in the inertial sub-region, proving that the $PM_{2.5}$ concentration fluctuation agrees with the Kolmogorov theory under certain conditions. The universal functions of $PM_{2.5}$ concentration $\varphi_c(\zeta)$ in relation to the stability parameter ζ for different regions were provided.

The COATS experiment revealed the influencing mechanisms of the ABL structure evolution on the vertical distribution of $PM_{2.5}$. The quantitative contribution of the ABL processes to pollutant transport and diffusion in different seasons was evaluated, which enriched our understanding of the turbulent transport of $PM_{2.5}$ between the ground and the atmosphere. Particularly, discoveries were made regarding the spatial structure heterogeneity of the ABL and its influence on the spatial distribution of pollutants, and a three-dimensional structural image of the ABL during haze pollution in the NCP was obtained. However, the studies on the quantitative influence and physical mechanisms of the ABL on pollutant transport during haze pollution, as well as on turbulent motion are still less sufficient. Future researches are suggested to further verify the turbulent transport mechanisms of pollutants based on the combination observations of boundary layer profiles and turbulence gra-

dient by meteorological tower. Research on the spatial structure of turbulence in the ABL shall be conducted to explore the influence of intermittent turbulence on pollutant diffusion and the turbulent transport law in the SBL. A universal flux-profile relationship for $PM_{2.5}$ concentrations and a turbulent diffusion coefficient needs to be developed and verified. Quantitative understandings of the interaction mechanisms between the ABL and haze pollution may be deepened with the help of numerical simulation studies, and the ABL parameterization schemes for a polluted atmosphere could be developed and modified based on the observation results so that the air quality forecasting level may be improved.

Acknowledgements *We sincerely thank the three anonymous reviewers for their constructive comments on the early version of the manuscript. This work was supported by the National Natural Science Foundation of China (Grant Nos. 42090031, 42175092, 92044301 & 91544216), the National Key R&D Program of China (Grant Nos. 2016YFC0203306 & 2017YFC0209600) and the National Research Program for Key Issues in Air Pollution Control (Grant Nos. DQGG0104 & DQGG0106).*

References

Banta R M, Newsom R K, Lundquist J K, Pichugina Y L, Coulter R L, Mahrt L. 2002. Nocturnal low-level jet characteristics over Kansas during Cases-99. Bound-Layer Meteor, 105: 221–252

Bei N, Zhao L, Xiao B, Meng N, Feng T. 2017. Impacts of local circulations on the wintertime air pollution in the Guanzhong Basin, China. Sci Total Environ, 592: 373–390

Bei N, Li X, Tie X, Zhao L, Wu J, Li X, Liu L, Shen Z, Li G. 2020. Impact of synoptic patterns and meteorological elements on the wintertime haze in the Beijing-Tianjin-Hebei region, China from 2013 to 2017. Sci Total Environ, 704: 135210

Cai S, Wang Y, Zhao B, Wang S, Chang X, Hao J. 2017. The impact of the "Air Pollution Prevention and Control Action Plan" on $PM_{2.5}$ concentrations in Jing-Jin-Ji region during 2012–2020. Sci Total Environ, 580: 197–209

Cao Z, Sheng L, Liu Q, Yao X, Wang W. 2015. Interannual increase of regional haze-fog in North China Plain in summer by intensified easterly winds and orographic forcing. Atmos Environ, 122: 154–162

Chen J, Zhao C S, Ma N, Liu P F, Göbel T, Hallbauer E, Deng Z Z, Ran L, Xu W Y, Liang Z, Liu H J, Yan P, Zhou X J, Wiedensohler A. 2012. A parameterization of low visibilities for hazy days in the North China Plain. Atmos Chem Phys, 12: 4935–4950

Collis R T H, Fernald F G, Ligda M G H. 1964. Laser radar echoes from a stratified clear atmosphere. Nature, 203: 1274–1275

Collis R T H, Ligda M G H. 1964. Laser radar echoes from the clear atmosphere. Nature, 203: 508

Deng Z Z, Zhao C S, Ma N, Ran L, Zhou G Q, Lu D R, Zhou X J. 2013. An examination of parameterizations for the CCN number concentration based on *in situ* measurements of aerosol activation properties in the North China Plain. Atmos Chem Phys, 13: 6227–6237

Fan H, Zhao C, Yang Y. 2020. A comprehensive analysis of the spatio-temporal variation of urban air pollution in China during 2014–2018. Atmos Environ, 220: 117066

Guo B, Wang Y, Zhang X, Che H, Zhong J, Chu Y, Cheng L. 2020. Temporal and spatial variations of haze and fog and the characteristics of $PM_{2.5}$ during heavy pollution episodes in China from 2013 to 2018. Atmos Pollution Res, 11: 1847–1856

Guo L J, Guo X L, Fang C G, Zhu S C. 2014. Observation analysis on characteristics of formation, evolution and transition of a long-lasting severe fog and haze episode in North China. Sci China Earth Sci, 58: 329–344

Han X, Zhang M, Zhu L, Skorokhod A. 2016. Assessment of the impact of emissions reductions on air quality over North China Plain. Atmos Pollution Res, 7: 249–259

Jin X, Cai X, Yu M, Song Y, Wang X, Kang L, Zhang H. 2020. Diagnostic analysis of wintertime $PM_{2.5}$ pollution in the North China Plain: The impacts of regional transport and atmospheric boundary layer variation. Atmos Environ, 224: 117346

Jin X, Cai X, Yu M, Wang X, Song Y, Kang L, Zhang H, Zhu T. 2021. Mesoscale structure of the atmospheric boundary layer and its impact on regional air pollution: A case study. Atmos Environ, 258: 118511

Jin X, Cai X, Yu M, Song Y, Wang X, Zhang H, Zhu T. 2022a. Regional $PM_{2.5}$ pollution confined by atmospheric internal boundaries in the North China Plain: Boundary layer structures and numerical simulation. Atmos Chem Phys, 22: 11409–11427

Jin X, Cai X, Yu M, Wang X, Song Y, Wang X, Zhang H, Zhu T. 2022b. Regional $PM_{2.5}$ pollution confined by atmospheric internal boundaries in the North China Plain: Analysis based on surface observations. Sci Total Environ, 841: 156728

Kanawade V P, Srivastava A K, Ram K, Asmi E, Vakkari V, Soni V K, Varaprasad V, Sarangi C. 2020. What caused severe air pollution episode of November 2016 in New Delhi? Atmos Environ, 222: 117125

Lee J, Hong J W, Lee K, Hong J, Velasco E, Lim Y J, Lee J B, Nam K, Park J. 2019. Ceilometer monitoring of boundary-layer height and its application in evaluating the dilution effect on air pollution. Bound-Layer Meteorol, 172: 435–455

Li G, Su H, Ma N, Tao J, Kuang Y, Wang Q, Hong J, Zhang Y, Kuhn U, Zhang S, Pan X, Lu N, Tang M, Zheng G, Wang Z, Gao Y, Cheng P, Xu W, Zhou G, Zhao C, Yuan B, Shao M, Ding A, Zhang Q, Fu P, Sun Y, Pöschl U, Cheng Y. 2021. Multiphase chemistry experiment in Fogs and Aerosols in the North China Plain (McFAN): Integrated analysis and intensive winter campaign 2018. Farad Discuss, 226: 207–222

Li J, Sun J, Zhou M, Cheng Z, Li Q, Cao X, Zhang J. 2018. Observational analyses of dramatic developments of a severe air pollution event in the Beijing area. Atmos Chem Phys, 18: 3919–3935

Li Q H. 2022. Effects of the spatial structure of the atmospheric boundary layer on haze pollution in the North China Plain: An experimental study (in Chinese). Doctoral Dissertation. Beijing: Peking University

Li Q H, Wu B G, Liu J L, Zhang H, Cai X H, Song Y. 2020. Characteristics of the atmospheric boundary layer and its relation with $PM_{2.5}$ during haze episodes in winter in the North China Plain. Atmos Environ, 223: 117265

Li Q, Zhang H, Cai X, Song Y, Zhu T. 2021. The impacts of the atmospheric boundary layer on regional haze in North China. NPJ Clim Atmos Sci, 4: 9

Li Q, Zhang H, Jin X, Cai X, Song Y. 2022. Mechanism of haze pollution in summer and its difference with winter in the North China Plain. Sci Total Environ, 806: 150625

Li R, Li Z, Gao W, Ding W, Xu Q, Song X. 2015. Diurnal, seasonal, and spatial variation of $PM_{2.5}$ in Beijing. Sci Bull, 60: 387–395

Li X, Hu X M, Ma Y, Wang Y, Li L, Zhao Z. 2019. Impact of planetary boundary layer structure on the formation and evolution of air-pollution episodes in Shenyang, Northeast China. Atmos Environ, 214: 116850

Liang X, Miao S, Li J, Bornstein R, Zhang X, Gao Y, Chen F, Cao X, Cheng Z, Clements C, Dabberdt W, Ding A, Ding D, Dou J J, Dou J X, Dou Y, Grimmond C S B, González-Cruz J E, He J, Huang M, Huang X, Ju S, Li Q, Niyogi D, Quan J, Sun J, Sun J Z, Yu M, Zhang J, Zhang Y, Zhao X, Zheng Z, Zhou M. 2018. SURF: Understanding and predicting urban convection and haze. Bull Am Meteorol Soc, 99: 1391–1413

Liu C, Huang J, Wang Y, Tao X, Hu C, Deng L, Xu J, Xiao H W, Luo L, Xiao H Y, Xiao W. 2020. Vertical distribution of $PM_{2.5}$ and interactions with the atmospheric boundary layer during the development stage of a heavy haze pollution event. Sci Total Environ, 704: 135329

Liu J, Fan S J, Wu D, Wu M, Liao Z H, Li H W. 2015. Boundary layer

characteristics of typical haze process in the Pearl River Delta region (in Chinese). China Environ Sci, 35: 1664–1674
Liu Q, Quan J, Jia X, Sun Z, Li X, Gao Y, Liu Y. 2019. Vertical profiles of aerosol composition over Beijing, China: Analysis of *in situ* aircraft measurements. J Atmos Sci, 76: 231–245
Liu X, Zhang Y, Jung J, Gu J, Li Y, Guo S, Chang S Y, Yue D, Lin P, Kim Y J, Hu M, Zeng L, Zhu T. 2009. Research on the hygroscopic properties of aerosols by measurement and modeling during CAREBeijing-2006. J Geophys Res, 114: D00G16
Ma N, Zhao C S, Nowak A, Müller T, Pfeifer S, Cheng Y F, Deng Z Z, Liu P F, Xu W Y, Ran L, Yan P, Göbel T, Hallbauer E, Mildenberger K, Henning S, Yu J, Chen L L, Zhou X J, Stratmann F, Wiedensohler A. 2011. Aerosol optical properties in the North China Plain during HaChi campaign: An *in-situ* optical closure study. Atmos Chem Phys, 11: 5959–5973
Miao Y, Liu S, Sheng L, Huang S, Li J. 2019. Influence of boundary layer structure and low-level jet on $PM_{2.5}$ pollution in Beijing: A case study. Int J Environ Res Public Health, 16: 616
Pan L, Xu J, Tie X, Mao X, Gao W, Chang L. 2019. Long-term measurements of planetary boundary layer height and interactions with $PM_{2.5}$ in Shanghai, China. Atmos Pollut Res, 10: 989–996
Peng H Q, Liu D Y, Zhao B, Su Y, Wu J M, Shen H, Wei J S, Cao L. 2016. Boundary-layer characteristics of persistent regional haze events and heavy haze days in eastern China. Adv Meteorol, 2016: 6950154, doi: 10.1155/2016/6950154
Qu Y, An J, Li J, Chen Y, Li Y, Liu X, Hu M. 2014. Effects of NOx and VOCs from five emission sources on summer surface O3 over the Beijing-Tianjin-Hebei region. Adv Atmos Sci, 31: 787–800
Quan J, Dou Y, Zhao X, Liu Q, Sun Z, Pan Y, Jia X, Cheng Z, Ma P, Su J, Xin J, Liu Y. 2020. Regional atmospheric pollutant transport mechanisms over the North China Plain driven by topography and planetary boundary layer processes. Atmos Environ, 221: 117098
Ran L, Zhao C S, Xu W Y, Lu X Q, Han M, Lin W L, Yan P, Xu X B, Deng Z Z, Ma N, Liu P F, Yu J, Liang W D, Chen L L. 2011. VOC reactivity and its effect on ozone production during the HaChi summer campaign. Atmos Chem Phys, 11: 4657–4667
Ren Y, Zhang H, Wei W, Wu B, Liu J, Cai X, Song Y. 2019a. Comparison of the turbulence structure during light and heavy haze pollution episodes. Atmos Res, 230: 104645
Ren Y, Zhang H, Wei W, Wu B, Cai X, Song Y. 2019b. Effects of turbulence structure and urbanization on the heavy haze pollution process. Atmos Chem Phys, 19: 1041–1057
Ren Y, Zhang H, Wei W, Cai X, Song Y. 2020. Determining the fluctuation of $PM_{2.5}$ mass concentration and its applicability to Monin-Obukhov similarity. Sci Total Environ, 710: 136398
Ren Y, Zhang H, Zhang X, Li Q, Cai X, Song Y, Kang L, Zhu T. 2021. Temporal and spatial characteristics of turbulent transfer and diffusion coefficient of $PM_{2.5}$. Sci Total Environ, 782: 146804
Shi Y, Hu F, Fan G, Zhang Z. 2019. Multiple technical observations of the atmospheric boundary layer structure of a red-alert haze episode in Beijing. Atmos Meas Tech, 12: 4887–4901
Shi Y, Hu F, Xiao Z, Fan G, Zhang Z. 2020. Comparison of four different types of planetary boundary layer heights during a haze episode in Beijing. Sci Total Environ, 711: 134928
Su T, Li Z, Kahn R. 2020. A new method to retrieve the diurnal variability of planetary boundary layer height from lidar under different thermodynamic stability conditions. Remote Sens Environ, 237: 111519
Silcox G D, Kelly K E, Crosman E T, Whiteman C D, Allen B L. 2011. Wintertime $PM_{2.5}$ concentrations during persistent, multi-day cold-air pools in a mountain valley. Atmos Environ, 46: 17–24
Sun H, Shi Y, Liu L, Ding W, Zhang Z, Hu F. 2021. Impacts of atmospheric boundary layer vertical structure on haze pollution observed by tethered balloon and lidar. J Meteorol Res, 35: 209–223
van Pinxteren D, Brüggemann E, Gnauk T, Iinuma Y, Müller K, Nowak A, Achtert P, Wiedensohler A, Herrmann H. 2009. Size- and time-resolved chemical particle characterization during CAREBeijing-2006: Different pollution regimes and diurnal profiles. J Geophys Res, 114: D00G09
Wang L, Gao Z, Miao S, Guo X, Sun T, Liu M, Li D. 2015. Contrasting characteristics of the surface energy balance between the urban and rural areas of Beijing. Adv Atmos Sci, 32: 505–514
Wang Z, Cao X, Zhang L, Notholt J, Zhou B, Liu R, Zhang B. 2012. Lidar measurement of planetary boundary layer height and comparison with microwave profiling radiometer observation. Atmos Meas Tech, 5: 1965–1972
Wang Z F, Li J, Wang Z, Yang W Y, Tang X, Ge B Z, Yan P Z, Zhu L L, Chen X S, Chen H S, Wand W, Li J J, Liu B, Wang X Y, Wand W, Zhao Y L, Lu N, Su D B. 2014. Modeling study of regional severe hazes over mid-eastern China in January 2013 and its implications on pollution prevention and control. Sci China Earth Sci, 57: 3–13
Wei W, Zhang H, Wu B, Huang Y, Cai X, Song Y, Li J. 2018. Intermittent turbulence contributes to vertical dispersion of $PM_{2.5}$ in the North China Plain: Cases from Tianjin. Atmos Chem Phys, 18: 12953–12967
Wei W, Zhang H, Cai X, Song Y, Bian Y, Xiao K, Zhang H. 2020. Influence of intermittent turbulence on air pollution and its dispersion in winter 2016/2017 over Beijing, China. J Meteorol Res, 34: 176–188
Whiteman C D, Bian X, Zhong S. 1999. Wintertime evolution of the temperature inversion in the Colorado Plateau Basin. J Appl Meteor, 38: 1103–1117
Wu Z, Wang Y, Tan T, Zhu Y, Li M, Shang D, Wang H, Lu K, Guo S, Zeng L, Zhang Y. 2018. Aerosol liquid water driven by anthropogenic inorganic salts: Implying its key role in haze formation in the North China Plain. Environ Sci Technol Lett, 5: 160–166
Xu T, Song Y, Zhang M, Liu M, Cai X, Zhang H, Tao Z, Pan Y, Zhu T. 2020. Investigation of the atmospheric boundary layer during an unexpected summertime persistent severe haze pollution period in Beijing. Meteorol Atmos Phys, 132: 71–84
Xu X D, Ding G A, Bian L G. 2006. Beijing city air pollution observation experiment (in Chinese). J Appl Meteorol Sci, 17: 815–828
Xu X D, Ding G A, Bian L G, Xie L A. 2004. Characteristics of atmospheric environment of boundary layer structure of city community in BECAPEX and integrate influence (in Chinese). Acta Meteorol Sin, 62: 663–672
Yang Y, Liu X, Qu Y, Wang J, An J, Zhang Y, Zhang F. 2015. Formation mechanism of continuous extreme haze episodes in the megacity Beijing, China, in January 2013. Atmos Res, 155: 192–203
Ye X, Song Y, Cai X, Zhang H. 2016. Study on the synoptic flow patterns and boundary layer process of the severe haze events over the North China Plain in January 2013. Atmos Environ, 124: 129–145
Yu M, Cai X, Xu C, Song Y. 2019. A climatological study of air pollution potential in China. Theor Appl Climatol, 136: 627–638
Zhang Q, Quan J, Tie X, Li X, Liu Q, Gao Y, Zhao D. 2015. Effects of meteorology and secondary particle formation on visibility during heavy haze events in Beijing, China. Sci Total Environ, 502: 578–584
Zhong J, Zhang X, Wang Y, Sun J, Zhang Y, Wang J, Tan K, Shen X, Che H, Zhang L, Zhang Z, Qi X, Zhao H, Ren S, Li Y. 2017. Relative contributions of boundary-layer meteorological factors to the explosive growth of $PM_{2.5}$ during the red-alert heavy pollution episodes in Beijing in December 2016. J Meteorol Res, 31: 809–819
Zhong J, Zhang X, Dong Y, Wang Y, Liu C, Wang J, Zhang Y, Che H. 2018a. Feedback effects of boundary-layer meteorological factors on cumulative explosive growth of $PM_{2.5}$ during winter heavy pollution episodes in Beijing from 2013 to 2016. Atmos Chem Phys, 18: 247–258
Zhong J, Zhang X, Wang Y, Liu C, Dong Y. 2018b. Heavy aerosol pollution episodes in winter Beijing enhanced by radiative cooling effects of aerosols. Atmos Res, 209: 59–64
Zou Q Q, Cai X H, Guo M T, Song Y, Zhang X L. 2018. Long-term mean footprint and its relationship to heavy air pollution episodes in Beijing (in Chinese). Acta Sci Nat Univ Pekin, 54: 341–349

(Responsible editor: Chao LIU)